GEOLOGIC HISTORY OF MAUNA LOA'S SUBMARINE SOUTHWEST RIFT ZONE (SWRZ)

A THESIS SUBMITTED TO THE GRADUATE DIVISION OF THE
UNIVERSITY OF HAWAI'I AT MĀNOA IN PARTIAL FULFILLMENT
OF THE REQUIREMENTS FOR THE DEGREE OF

MASTER OF SCIENCE
IN
GEOLOGY AND GEOPHYSICS

DECEMBER 2012

By
Darwina K. Griffin

Thesis Committee:

Scott K. Rowland, Chairperson
Michael O. Garcia
Frank A. Trusdell

Keywords: Mauna Loa, submarine rift zones, submarine landslides

ACKNOWLEDGEMENTS

I would like to thank my advisor, Scott K. Rowland, for his support, guidance, and most importantly, for his patience throughout the years. A special thank you to Frank A. Trusdell, for being a great mentor for the past decade, for sharing with me his knowledge of Mauna Loa volcano, and for pitching the idea to me to take on this project. I owe him a lot of beers. I would also like to thank Michael O. Garcia. I would not have been a graduate student at SOEST without his help. Again, this manuscript would not have been completed without all of my committee members' discussions, comments, and reviews.

A special thank you to Julie Herrick, Malin Klawonn, and Melanie Abecassis for last minute reviews of the manuscript! To Tracy Ibarra, Hadley Nunes, Beatrice Clyde-Smith, Thomas Shea, Clara Margalef Folque, Michele Harman, Daisy Wheeler, Jess Wardlaw, Lynne Fagents, Andrea Steffke, the Horsemen, Krystian Paczkowski, Jessica Barnes, Elise Rumpf, Ashton Flinders, and Lisa Swinnard for additional support (e.g., defense preparation, brunch and phone dates, coffee breaks, and surf lessons) while I was in the thick of it. Also, thank you to my friends (especially from the BI), past office husbands/wives, and professors for enriching my experience as a graduate student.

Big Mahalo to James Cave and Carolina Anchieta Fermin for keeping me sane during the final weeks of thesis life. I am so grateful for their compassion and for the 2nd and 3rd home/office that they shared with me.

Finally, thank you to my family for their overwhelming love and support and to my Dad for proofreading my manuscript. It has been a journey with many detours.

ABSTRACT

Using a combination of high spatial (~30 m) resolution multi-beam bathymetry and backscatter data collected in 2002, and underwater video footage and still images collected by Jason, we present a new geologic map and interpretations of the geologic history of Mauna Loa's submarine southwest rift zone (SWRZ). This study provides new insights on why the SWRZ's Western and Eastern flanks differ. The Western flank was sculpted by at least four stages of flank collapse, followed by ongoing volcanic activity and depositional processes (i.e., volcaniclastics generated by ocean entries). In contrast, the Eastern flank is distinctively rugged due to abundant constructional features (i.e., volcanic cones and pillow mounds). In addition, there is no clear evidence of any recent volcanism, suggesting that this portion of the flank has been inactive for quite some time.

TABLE OF CONTENTS

LIST OF TABLES

LIST OF FIGURES

CHAPTER 1. INTRODUCTION

The island of Hawai‘i, located at the southeast end of the Hawaiian-Emperor Seamount chain in the Pacific Ocean, is made up of five coalesced shield volcanoes: Kohala, Mauna Kea, Hualālai, Mauna Loa, and Kīlauea (Fig. 1). Two additional volcanoes, Lō‘ihi and Mahukona, are on the flanks of the island (Fig. 1). Mauna Loa is the world's largest volcano (Lipman, 1980; Lockwood and Lipman, 1987). It rises from nearly 5,000 m below sea level (m.b.s.l) to 4,169 m above sea level (m.a.s.l; Lipman, 1980; Lockwood and Lipman, 1987). With the underlying oceanic crust depressed by an additional 8,000 m (Zucca et al., 1982; Hill and Zucca, 1987), the total volume has been estimated to be ~75,000 km^3 (e.g., Robinson and Eakins, 2006).

Since the first Europeans arrived in Hawai‘i in the late 1770s and the start of the volcano's written record, Mauna Loa has erupted at least 33 times (e.g., Lockwood and Lipman 1987; Barnard, 1995; Trusdell, 1995). Of these eruptions, six produced extensive lava flows that crossed the shoreline: 1859, 1868, 1887, 1919, 1926, and 1950 (Figs. 1, 4). Mauna Loa last erupted in 1984.

Mauna Loa eruptions commonly take place in or near the summit caldera, Moku‘āweoweo, or along the two rift zones extending to the northeast and southwest (Fig. 1; Lipman, 1980; Lockwood and Lipman, 1987). From the summit to ~5,000 m.b.s.l the southwest rift zone (SWRZ) is ~100 km in length (Fig. 1). By comparison, the northeast rift zone (NERZ) dies out about ~50 km from the summit caldera (Fig. 1; e.g., Lipman 1980; Trusdell et al., 2006). Unlike other Hawaiian volcanoes, Mauna Loa also erupts from radial vents located on its northern and western flanks (Fig. 1; e.g.,

Lipman, 1980; Lockwood and Lipman, 1987; Wolfe and Morris, 1996; Trusdell et al., 2006; Wanless et al., 2006). Lockwood and Lipman (1987), Wanless et al. (2006), and Trusdell (2012) identified 66, 44, and 45 vents respectively.

Mauna Loa's subaerial surface flows, which cover an area >5,000 km^2, have been mapped multiple times (e.g., Stearns, 1930; Stearns and Macdonald, 1946; Lipman and Swenson, 1984; Lockwood and Lipman, 1987; Wolfe and Morris, 1996; Trusdell et al., 2006; Trusdell and Lockwood, 2006; Trusdell and Lockwood, 2009; Trusdell and Lockwood, in review). The recent mapping efforts were supported by age dating using radiocarbon (^{14}C), K-Ar, and Ar-Ar methods (e.g., Lockwood and Lipman, 1987; Lipman, 1995; Lockwood, 1995; Trusdell et al., 2006; Pressling et al., 2009; Jicha et al., 2012). Collectively these efforts have allowed us to gain a better understanding of Mauna Loa's Holocene eruptive history (e.g., Lockwood and Lipman, 1987; Lockwood, 1995; Trusdell et al., 2006, Trusdell, 2012). The geologic record, however, remains incomplete because it does not include the bulk of the volcano which lies under the surface and/or underwater (e.g., Walker, 1990; Lockwood, 1995; Trusdell et al., 2006, Trusdell, 2012).

In this thesis high spatial resolution bathymetry, backscatter data, and underwater video footage and photographs collected in 2002 were analyzed to create a geologic map of Mauna Loa's submarine SWRZ and adjacent areas. From this map we attempt to interpret the geologic history of these submarine flanks. The results provide insights into Mauna Loa's overall history, which is crucial to understanding how the volcano has evolved. Because Mauna Loa is an archetype of basaltic shield volcanism, what we learn about its growth may be applied towards the study of other Hawaiian volcanoes.

1.1. Previous Work

1.1.1. Subaerial Geologic Record

It is thought that Mauna Loa has been active for the past 0.6-1.0 Ma (e.g., Moore and Clague, 1992; Lipman, 1995). The mapped geologic record of Mauna Loa accounts for only a small portion of the volcano's history and is based almost exclusively on its subaerial exposures. Approximately 98% of these surface exposures are lava flows and ash deposits younger than 10 ka (Lockwood, 1995).

Subaerial volcanic units on Mauna Loa are categorized into three main groups: the Nīnole Basalt, the Kahuku Basalt, and the Kaʻū Basalt (e.g., Stearns and Macdonald, 1946; Lipman and Swenson, 1984; Wolfe and Morris, 1996; Trusdell et al., 2006). The oldest exposed rocks on the subaerial flanks of Mauna Loa belong to the Nīnole Basalt which forms the Nīnole Hills (Figs. 1, 2). They are a series of steep-sided hills isolated by deep erosional valleys and their origin to this day remains enigmatic (e.g., Lipman et al., 1990; Trusdell et al., 2006).

Some studies considered the Nīnole Hills to be remnants of an older volcano that was later partially buried by lavas from Mauna Loa (e.g., Stearns and Clark, 1930; Stearns and Macdonald, 1946). It has been suggested that they are remnants of an old Mauna Loa flank that has been displaced within the Kaʻōiki-Honuʻapo fault system (Fig. 1; Lipman, 1980). The Nīnole Hills may also be eruptive products from an early southwest (or south) rift zone of Mauna Loa (Lipman et al., 1990). Rocks exposed in the hills are estimated to be ~100 to 200 ka old (Lipman et al., 1990). Jicha et al. (2012) present new age estimates of ~108 to 227 ka for the Nīnole Hills.

The rest of subaerial Mauna Loa consists of the Kahuku and Kaʻū Basalts, which respectively are below and above the Pāhala Ash (Lipman and Swenson, 1984; Wolfe and Morris, 1996). The Pāhala Ash is a distinct unit made up of deeply weathered basaltic ash. On the southeastern flanks of Mauna Loa this unit can be as much as 10 m thick (Lipman and Swenson, 1984). Near the town of Nāʻālehu one of the lava flows belonging to the Kaʻū volcanics overlying the Pāhala Ash yields a radiocarbon age of 31,000 ± 900 ka (Lipman and Swenson, 1984). The Kaʻū Basalt includes all post-Pāhala Ash (i.e., younger than 31 ka) lavas and pyroclastics (Lipman and Swenson, 1984; Wolfe and Morris, 1996).

1.1.1.1. Kealakekua and Kahuku Palis and Mokuʻāweoweo

Pre-Holocene subaerial exposures on Mauna Loa volcano are rare, limited in thickness, and usually weathered. These are best exposed along palis - Hawaiian for cliff - such as the Kealakekua Pali and the Kahuku Pali (Figs. 1, 3-5; e.g., Lipman and Swenson, 1984; Wolfe and Morris, 1996; Trusdell et al., 2006). These palis are normal fault scarps formed by downward displacement of the seaward part of the west flank (e.g., Lipman, 1980). Farther inland the height of these palis decreases as they are buried by younger lava flows.

The Kealakekua Pali is located on the west flank of Mauna Loa (Figs. 1, 3, 5). Movement along this fault has left a seaward facing scarp up to 500 m high (Moore and Chadwick, 1995). With K-Ar dating methods, three lava flows dated ~185 m below the top of the stratigraphic section yield a weighted mean age of 166 ± 53 ka (Lipman, 1995). Two samples obtained from a bright red ash zone in the pali, however, yield ages of 31

ka (Lockwood, 1995) and 36 ka (F.A. Trusdell, oral commun., 2008) inconsistent with the data of Lipman (1995). This inconsistency is yet to be explained.

The Kahuku Pali extends north from Ka Lae, the southernmost point on Hawai‘i. Along this pali, relief can be as much as 200 m (Figs. 1, 4; Macdonald et al., 1983). Attempts to date lava flows from this section with K-Ar dating techniques have been unsuccessful due to alteration, low K, and excess Ar (Lipman, 1995). In Moku‘āweoweo, the summit caldera, rocks exposed along the walls are all <3,500 ka old (F.A. Trusdell, oral commun., 2007).

1.1.2. Submarine Geologic Record

As remote sensing techniques have become more advanced, and oceanographic explorations more frequent, information about Mauna Loa's submarine flanks has become available. These flanks, which descend to ~5,000 m.b.s.l have been studied by numerous investigators. Areas investigated recently include the submarine flanks west (e.g., Wanless et al., 2006) and northwest (e.g., Lipman and Coombs, 2006) of Kealakekua Bay. Mauna Loa's submarine flanks south-southwest of Ka Lae have also been examined (e.g., Fornari et al., 1979; Garcia et al., 1995; Moore and Chadwick, 1995).

1.1.2.1. Landslides

In 1983 the United States declared an Exclusive Economic Zone (EEZ) extending from the coastline to 200 nautical miles offshore. In response to this, the U.S. Geological Survey partnered with the British Institute of Oceanographic Sciences (IOS) to map the

seafloor surrounding the Hawaiian Islands (Groome et al., 1997). GLORIA (Geologic Long-Range Inclined Asdic), a sidescan sonar mapping system developed by the IOS was used to complete the first comprehensive study of the seafloor around Hawai‘i.

Abundant giant submarine landslides were identified on the flanks of the Hawaiian volcanoes (e.g., Moore et al., 1989; Moore et al., 1994; Groome et al., 1997; Holcomb and Robinson, 2004). Since then, the submarine landslides on the flanks of Mauna Loa have been examined in greater detail. Generally these are classified into two major groups: debris avalanches and slumps.

Debris avalanches are the result of catastrophic events. Examples include the East and West Ka Lae debris avalanches and the ‘Ālika 1 and 2 debris avalanches (Fig. 5; Table 1; e.g., Moore and Chadwick, 1995). Slumps, on the other hand, are inferred to be slow moving masses because internally they are largely undeformed. Examples include the North Kona slump and the South Kona slide complex (Fig. 5; Table 1; e.g., Lipman et al., 1988; Moore et al., 1994; Moore et al., 1995; Moore and Chadwick, 1995; McMurtry et al., 1999; Yokose and Lipman, 2004; Lipman and Coombs, 2006). The types and ages of slumps and debris avalanches on the submarine flanks of Mauna Loa are listed in Table 1.

Detailed studies of these large mass-wasting features (e.g., Lipman et al., 1988; Moore et al., 1994; Moore et al., 1995; Moore and Chadwick, 1995; McMurtry et al., 1999; Yokose and Lipman, 2004; Lipman and Coombs, 2006) and offshore maps of Hawai‘i and adjacent islands (Moore and Chadwick, 1995; Eakins et al., 2003; Holcomb and Robinson, 2004) demonstrate that slope failures are common on Mauna Loa. These studies have shown that large-scale mass-wasting takes place throughout the volcano’s

shield building stage. Because several debris avalanches have been identified on the submarine flanks of Lō‘ihi volcano, mass-wasting may have been an important process during Mauna Loa’s pre-shield stage as well (e.g., Moore and Chadwick, 1995).

1.1.2.2. Scarps

Submarine landslides provide ideal areas to study Mauna Loa’s early history. They expose in their scarps flows that are similar in age or older than, the 100-227 ka Nīnole Basalts (e.g., Lipman et al., 1990; Garcia et al., 1995; Lipman, 1995; Jicha et al., 2012). In particular, the submarine extension of the Kahuku Pali, a prominent west-facing scarp with relief as great as 1,900 m, has been surveyed offshore from Ka Lae (e.g., Fornari et al., 1979; Chadwick et al., 1993; Garcia et al., 1995).

Work by Fornari et al. (1979), Moore et al. (1989), Moore and Clague (1992), Chadwick et al. (1993), Moore et al. (1994), and Garcia et al. (1995) suggests that the East Ka Lae debris avalanche is responsible for the submarine Kahuku Pali. It has been inferred that both the East and West Ka Lae debris avalanches are younger than the ‘Ālika 1 and 2 debris avalanches based on their appearances in GLORIA images (Moore and Clague, 1992). The youngest pillow lava sampled from the scarp section suggests a maximum age of ~120 ka for the East Ka Lae debris avalanche (Jicha et al., 2012). It has also been suggested that this avalanche could be younger (i.e., ~30 ka; Moore et al., 1990).

Lipman et al. (1990), Lipman (1995), and Garcia et al. (1995) assumed that lavas exposed in the submarine Kahuku Pali are older than any of those exposed in the subaerial Kahuku Pali. Their age estimates for these submarine lavas are 100-350 ka

(Garcia et al., 1995; Lipman, 1995). Jicha et al. (2012) give an older age of ~470 ka based on lavas sampled from a ~1.3 km vertical section of the scarp face.

1.1.2.3. Island Subsidence

As Hawaiian volcanoes age they also undergo subsidence, eventually becoming seamounts as the Pacific plate, which they are built upon, moves away from the hotspot towards the Kurile-Kamchatka and Aleutian trenches to the northwest. This relationship is best illustrated by looking at the entire length of the Hawaii-Emperor volcanic chain. Volcanoes of the chain get progressively older (as old as 75-80 Ma; e.g., Clague and Dalrymple, 1987; 1989) to the northwest. At the northwestern end of the chain, their summits are a few kilometers beneath the sea level (e.g., Clague and Dalrymple, 1987; Walker, 1990; Moore and Clague, 1992). Moving southeastward, between Gardner Pinnacle and Ni‘ihau, older volcanoes are not entirely submerged, but are present as small volcanic islets and coral atolls (e.g., Clague and Dalrymple, 1987). The main Hawaiian Islands, even though they stand well above sea level, show extensive evidence of subsidence. In bathymetry, the most obvious indicators are prominent submarine terraces which surround the islands (e.g., Fornari and Campbell, 1987; Mark and Moore, 1987; Moore, 1987; Moore and Chadwick, 1995; Eakins et al., 2003; Holcomb and Robinson, 2004).

Hawaiian volcanoes subside over time for a number of reasons. The Pacific plate undergoes thermal aging and as the lithosphere moves away from the hot spot, it cools, thickens, and sinks (e.g., Clague and Dalrymple, 1987). Moreover, the volcanic loads cause the lithosphere to flex downward, resulting in additional subsidence (e.g., Zucca et

al., 1982; Clague and Dalrymple, 1987; Hill and Zucca, 1987; Moore, 1987; Walker, 1990; Moore and Clague, 1992).

The subaerial slopes of Hawaiian volcanoes during the shield-building stage are gradual (e.g., Mark and Moore, 1987; Walker, 1990). Gentle slopes result primarily because tholeiitic basalt flows erupting at the surface have low viscosities, and thus are able to travel far from their source vents. Mauna Loa's subaerial slopes that have not been modified by fault scarps or erosion are mostly gentle. Slopes are generally steeper at higher elevations and near the summit Moku'āweoweo they are rarely >10-11º (Mark and Moore, 1987; Rowland and Garbeil, 2000). At lower elevations, from <2,000 m.a.s.l to the shoreline, slopes are between 3-6º with an average of about 4º (Mark and Moore, 1987; Rowland and Garbeil, 2000).

In contrast to the subaerial slopes, submarine slopes tend to be steeper, especially just offshore (e.g., Mark and Moore, 1987; Moore, 1987; Walker, 1990; Moore and Chadwick, 1995; Eakins et al., 2003; Holcomb and Robinson, 2004). According to Mark and Moore (1987), slopes of Mauna Loa steepen from <5° at the coast to ~13° down at ~500 m.b.s.l. The difference in slope immediately above and below sea level, therefore, creates a distinct break in slope. For older Hawaiian volcanoes, these now-submerged slope breaks, mark former shorelines at the time that the volcano ended its main shield-building phase, i.e., when shoreward building could no longer keep up with subsidence (e.g., Mark and Moore, 1987; Moore, 1987; Walker, 1990; Moore and Clague, 1992; Garcia et al., 1995; Moore and Chadwick, 1995; Eakins et al., 2003; Holcomb and Robinson, 2004). By knowing the depths at which these slope breaks (or former shorelines) occur we are able to learn about how much subsidence volcanoes have

undergone since the slope breaks were created (e.g., Mark and Moore, 1987; Moore, 1987; Moore and Clague, 1992).

On Mauna Loa's western and southern flanks, offshore of Kealakekua Bay and Ka Lae respectively, there are two prominent submarine terraces and they are believed to correlate with each other (e.g., Moore et al., 1990; Moore and Clague, 1992; Chadwick et al., 1993; Garcia et al., 1995; Moore and Chadwick, 1995; Holcomb and Robinson, 2004; Webster et al., 2004). Submersible dives and bathymetric surveys of the Ka Lae terrace verified that it is a reef terrace (Moore et al., 1990; Garcia et al., 1995). Extending from Ka Lae to Laeokamilo Point, the terrace slopes gently seaward, at a depth range of 160-180 m.b.s.l it ends at a break in slope (Moore et al., 1990; Chadwick et al., 1993; Garcia et al., 1995). Moore et al. (1990) observed reef outcrops in water as deep as ~280-300 m.b.s.l and shallower than 160 m.b.s.l. Garcia et al. (1995) noted a dead coral reef outcrop between 165-190 m.b.s.l.

Coral reefs grow on the flanks of Hawaiian volcanoes when conditions permit, for example, during a period of waning volcanic activity when lava flows no longer (or rarely) enter the ocean (e.g., Moore and Clague, 1992; Moore and Chadwick, 1995). This waning volcanic activity, combined with sea level falling eustatically at rates comparable to island subsidence creates shallow environments that are favorable places for coral reefs to grow and be preserved (e.g., Moore, 1987; Mark and Moore, 1987; Moore et al., 1990; Moore and Clague, 1992; Garcia et al., 1995; Moore and Chadwick, 1995). With a vertical growth rate of ~10-20 mm/yr (e.g., Moore and Chadwick, 1995; Montaggioni et al., 1997; Webster et al., 2004), coral reefs are able to keep pace with continued

subsidence of Hawai‘i island, a rate estimated to be between 2.4-2.6 mm/yr (e.g., Moore, 1987; Moore et al., 1990).

Based on the slope break depth of 160 m.b.s.l and an assumed constant subsidence rate of 2.6 mm/yr (Moore et al., 1990), Garcia et al. (1995) suggest that there has been little volcanic activity along this portion of Mauna Loa's SWRZ for the past ~60 ka. Moore et al. (1990) and Webster et al. (2004) used ^{14}C and U-series techniques to date coral samples of the reef terrace and derived ages of 13-16 ka. Therefore, although Mauna Loa was and continues to subside, between ~60 ka and 13-16 ka, sea level must also have been dropping in order for the reef to have not drowned.

Moore et al. (1990) attributed drowning of the reef to the combined effects of island subsidence and rapid sea level rise at the end of the last glaciation. Webster et al. (2004) argued that drowning was primarily associated with unusually rapid sea level rise during the last deglaciation at around 15 ka (referred to as meltwater pulse 1A or MWP-1A). MWP-1A, a feature of the postglacial eustatic sea-level history, is characterized by unusually rapid sea level rise of about 40-50 mm/yr between 14.2-14.7 ka (Peltier, 2002; Webster et al., 2004). A reef with a vertical growth rate of ~10-20 mm/yr would have been unable to keep pace in both situations and as a result eventually drowned (Moore et al., 1990; Montaggioni et al., 1997; Webster et al., 2004).

Regions believe to have been at or near sea level in the past are also present at 425-450, 500, and 750 m.b.s.l. At ~ 425-450 m.b.s.l Moore et al. (1990) and Garcia et al. (1995) encountered an outcrop of large rounded boulders. Both Moore et al. (1990) and Garcia et al. (1995) interpreted this outcrop as a drowned boulder beach. Based on east-west bathymetric profiles of Mauna Loa's SWRZ ridge, Moore et al. (1990) proposed

that the crest of the ridge appears to be flat at 500 m.b.s.l and at 750 m.b.s.l, whereas at greater depths the ridge is steeper. Using depths of 500 m.b.s.l and 750 m.b.s.l, a subsidence rate of 2.5 mm/yr, and sea level data from Imbrie et al. (1984), Moore et al. (1990) suggested that along this portion of the rift zone there has been little volcanic activity in the past 170-270 ka. Preservation of the 13-16 ka reef, the slope break (160 m.b.s.l), boulders (425-450 m.b.s.l), and flat regions (500 and 750 m.b.s.l) have led Moore et al. (1990) and Garcia et al. (1995) to conclude that perhaps this portion of the submarine SWRZ has been extinct for the past tens of thousands of years.

1.1.3. Mauna Loa Submarine SWRZ - Present Day Morphology

The Western and Eastern flanks of Mauna Loa's submarine SWRZ differ considerably with respect to morphological texture and slope (Figs. 6, 13-16). The Western flank consists of three or four broad and relatively smooth-surfaced areas that in general slope <5° seaward. This area, referred to here as the Kahuku Gap (W3), is bounded on its eastern and western sides by two prominent scarps (W4 and W1 respectively) that have relief on the order of hundreds of meters to almost 2 kilometers. The east-facing scarp (W4) is part of the west flank of a large seaward-sloping block (the West-flank block; W4 and W5; Fig. 6). In contrast, the Eastern flank consists of multiple irregularly shaped and rugged-surfaced bathymetric highs (e.g., ridges and constructional features) separated by small scarps and valley-like features.

CHAPTER 2. METHODS

2.1. Data Collection

2.1.1. Bathymetry and Backscatter Data

In October and November of 2002, the submarine SE and SW flanks of Mauna Loa were surveyed by researchers from Universities Hawai‘i, Massachusetts, British Columbia, France, and Australia who teamed up with colleagues from Woods Hole Oceanographic Institute and the US Geological Survey aboard the R/V Thomas Thompson using the Kongsberg Simrad EM300 multi-beam sidescan sonar system. The hull-mounted EM300 system simultaneously collected high spatial resolution bathymetry and acoustic backscatter data from 1-40 km offshore, starting at Kealakekua Bay and extending to Punalu‘u (Figs. 1, 6). The 30 kHz multi-beam system was designed to map the seafloor from water as shallow as 10 m.b.s.l to as deep as 5,000 m.b.s.l (Kongsberg Maritime, 2003). This system can use up to 135 individual beams with beam-widths ranging from 1-4° (Kongsberg Maritime, 2003). The beam pointing angles depend on the water depth and are adjusted by the operator to maximize the number of usable beams. For detailed information and specifications on the EM300 system, refer to Kongsberg Maritime (2003) or the Woods Hole Oceanographic Institution (WHOI) website at http://www.whoi.edu/science/instruments.

The EM300 system’s transducer emits pulses of acoustic energy to the seafloor. Echoes that are reflected back are then recorded and used to determine bathymetry and backscatter. Depths are calculated using phase and amplitude detection (e.g., Torresan

and Gardner, 2000; Kongsberg Maritime, 2003). Backscatter values are obtained by measuring the amplitude of the echoes (e.g., Torresan and Gardner, 2000; Kongsberg Maritime, 2003). The EM300 system corrects for the effects of variable sound velocity and ship attitude (i.e., roll, pitch, and yaw; Kongsberg Maritime, 2003).

The EM300 vertical and horizontal accuracy is ~ 2.0% and ~0.2% of the water depth respectively (Kongsberg Maritime, 2003; Morgan et al., 2003). On the R/V Thomas Thompson, navigation was provided by precision code (P-code) GPS. The bathymetry data were collected at a ship speed of 8-10 knots. These bathymetry data are available at the Marine Geoscience Data System website at http://www.marine-geo.org/ under expedition TN151.

2.1.2. Jason Dive Data

In conjunction with seafloor mapping, underwater video footage and ocean-bottom still photographs were taken by Jason, a two-body remotely operated vehicle (ROV) built by the Deep Submergence Laboratory at WHOI. Jason is tethered to the ship with a 10 km-long fiber-optic cable and can dive to ~6,500 m.b.s.l (WHOI website). Jason dives typically last ~20 hours and during dives live video imagery and scientific data (i.e., navigation, depth, date, time, and event data) are fed back to the ship in real-time.

Six Jason dives were completed in Mauna Loa's submarine SWRZ area (Figs. 1, 6). These dives, J-16, -19, -20, -23, -24, and -25, collected ~90 hours of underwater video footage. The still images of the seafloor were collected at a rate of approximately 3 per minute for a total of more than 180,000 photographs. These still images are available

at the WHOI website http://4dgeo.whoi.edu/jason, under Hawaii 2002, cruise tn151. Unfortunately, however, these dataset cover only <<1 % of the field area. These videos and images were examined in detail because they serve as ground-truth for surface geology. Visual datasets facilitated characterization of the seafloor and allowed a better understanding of how surface cover such as sediment, talus, and lava flows changed with respect to geological features.

2.2. Data Analysis

2.2.1. Bathymetry

Most of the image processing and analysis of the bathymetric data was conducted with ArcGIS 9.x and ArcView GIS 3.3 software, developed by the Environmental Systems Research Institute (ESRI). Spatial Analyst extensions for these programs provided the necessary tools to create a number of morphologic datasets and maps such as bathymetric contours, slope, shaded-relief, and aspect from bathymetry. Individually, each map displayed different seafloor characteristics and when all were combined, helped to classify the seafloor into regions exhibiting spatially contiguous surface patterns. Each derived dataset is described below, with examples of how they contributed to understanding Mauna Loa's submarine SWRZ morphology.

2.2.1.1. Bathymetric Contours

To begin analysis, several maps with different bathymetry contour intervals were generated. Contour lines were essential because they allowed features such as ridges and

valleys, volcanic cones, and landslide scarps to be distinguished. Once these features were identified, detailed geomorphic observations were made. More than one bathymetric contour dataset was commonly used because analyses required different levels of detail. For example, to identify and analyze constructional features with relief >100 m (i.e., volcanic cones), a contour interval of 100 m is sufficient and does not result in a line density that is too great on steep slopes. Obviously, to identify and analyze features that are smaller than 100 m would require utilizing contour intervals of <100 m.

A number of constructional features were recognized in the study area that show the same characteristics of pointed/steep-sided and flat-topped cones that have been mapped on Mauna Loa's submarine west flank next to Kealakekua Bay (Wanless et al. 2006) and along other Hawaiian submarine rift zones (e.g., Clague et al., 2000). Based on observations made by Clague et al. (2000), D. Smith et al. (2002), J. Smith et al., (2002), Ren et al. (2004), Robinson and Eakins (2006), and Wanless et al. (2006), for example, there are several criteria that have to be met in order for a feature to be defined as a volcanic cone. These include: (1) the feature must have at least one closed contour when the contour interval is 20 m (2) the feature must be nearly circular or semi-circular in map view, or steep-sided and elongate (3) and the feature must have a relief above the surrounding seafloor of at least 50 m. Figure 7 is an example of a well-defined flat-topped cone. With GIS, information about the feature such as its depth, shape, and texture (e.g., wide spacing vs. close spacing; irregular vs. uniform), using various contour intervals were acquired easily. The cone is approximately 300 m high and its summit is centered at approximately ~2,825 m.b.s.l. It is nearly circular in shape and is relatively

planar. Shallow depressions are present at the summit. The flanks of the cone are rugged and steep (Fig. 7).

Another advantage of using GIS for analysis is the ability to overlay bathymetric contour lines on other morphologic datasets such as backscatter, slope, shaded-relief, and aspect (Figs. 7-12). Juxtaposing these different derivative datasets with contours allows relationships between datasets to be examined, contributing to insights about bathymetric features and/or regions being analyzed. To estimate the height of the flat-topped cone, slope, aspect, and bathymetric contours were juxtaposed (Figs. 7-11). Slope and aspect datasets are particularly helpful in determining the base of the cone's southern side where changes in slope (i.e., contour line density) are unclear compared to the cone's northeastern-southeastern side.

2.2.1.2. Shaded-relief

A shaded-relief image, also known as a hillshade map, represents topography and bathymetry with shades of gray (vary depending on the orientation of a slope with respect to the illumination direction), brightness and shadows. Eight shaded-relief images with illumination azimuths starting at 0° (due North) and going clockwise in increments of 45° were used for analysis. For all shaded-relief images a vertical illumination angle of 45º (the ArcGIS default) was applied. In each of the shaded-relief images, shapes and textures of seafloor features are either accentuated or subdued, depending on whether they are oriented perpendicular or parallel, respectively, to the illumination direction. Different illuminations highlight subtle differences in bathymetry, enhancing the ability

to discriminate features and/or regions, for example, which can be interpreted to be due to constructional/volcanic processes or mass-wasting processes.

The same flat-topped cone in Figure 7 is illuminated from the SE and SW respectively in Figures 8a and 8b. The two images demonstrate that the cone's summit and sides have differing surface textures. In both, the summit appears to be relatively smooth with little variation in brightness and shadows. The cone's flanks when illuminated from different angles, display variable brightness and shadows. This surface pattern indicates that the cone's flank is rugged.

2.2.1.3. Slope

Slope values in the study area derived from bathymetry range from horizontal (0°) to nearly vertical (~85°). Figures 9a and 9b present two ways of displaying the slope data. In Figures 9a, c, and d the slope values have been grouped into 8 classes using the Natural Breaks (Jenks) classification method. The resulting slope classes have increments of ~5º for slopes ranging from 0º-25º, and >5º for slopes >25º. Figure 9b, on the other hand, shows slope values stretched along a gray scale. Steep slopes are dark and gradual slopes are light. Classified slope data are especially useful for enhancing specific slope value ranges, and thus, were used for interpreting boundaries for features such as their bases and summits. Figure 9b also shows variations in steepness, but slope changes are more subdued. Both slope datasets give a sense of surface ruggedness and/or smoothness.

2.2.1.4. Aspect

Aspect is the dip direction of a slope. Values are given in degrees and start from 0° (North) and increase in a clockwise direction to 360º, where it is again due North. Aspect data were particularly useful in the mapping process for delineating features and regions. Aspect patterns occasionally highlight information about the study area that is not obvious in other datasets. For example, in Figure 10 the irregular aspect pattern shows that the surface of the summit dips in many directions. This observation suggests that microbathymetry exists on the summit of the flat-topped cone and that it is not entirely featureless. From bathymetric contours (Fig. 7), slope data (Figs. 9), or shaded-relief (Figs. 8) this information about the surface of the summit is not apparent or is not as pronounced.

2.2.2. Backscatter Data

Acoustic backscatter imagery depicts surface roughness and is frequently used to distinguish surfaces with high sediment cover (smooth) from surfaces with low sediment cover (rough) (e.g., Groome et al., 1997; Holcomb and Robinson, 2004; Chadwick et al., 2005; Wanless et al., 2006). Wanless et al. (2006) used backscatter data to map a number of relatively young submarine lava flows, and for some of the lava flows, their source vents (Wanless et al., 2006). Backscatter is used here in combination with other morphologic datasets to infer surface roughness of mapped regions and their features. In this thesis, high acoustic reflectivity is displayed in the sidescan imagery as white and low reflectivity as black, with a continuous gradient in-between.

In Figure 11, the summit of the flat-topped cone is characterized by low backscatter whereas the flanks have slightly higher backscatter and appear mottled. Shaded-relief (Figs. 8) and slope (Figs. 9) datasets of the cone show that the summit is relatively smooth and featureless. Aspect shows that the summit is not uniformly flat or featureless. It's surface, although appears smooth and featureless in shaded-relief and slope respectively, faces multiple directions in aspect (Fig. 10). Backscatter data show this surface overall has low backscatter intensities (Fig. 11). From all of the observations above, the summit can be interpreted to be slightly uneven with a heavy sediment cover.

Backscatter analysis also brought attention to several high backscatter areas that are low-relief areas in bathymetry (Figs. 12). Figure 12c shows that backscatter intensities for these areas are medium to high, thus they appear distinctively brighter than the surrounding seafloor, forming sharp boundaries. These bright (in backscatter) low-relief (in bathymetry) areas are interpreted to be surfaces that are younger than the dark seafloor surrounding them. These features are described in greater detail in the following chapter.

2.2.3. Jason Dive Data

Jason dive data (Figs. 1, 6) consist of underwater video footage, photographs, and a spreadsheet of attributes corresponding to the still images. Each data point is associated with three still images or video frames. Data point attributes used for analysis include latitude, longitude, date, time, depth, and logged notes. Date and time were helpful in correlating video footage to still images. To begin analysis and classification of these

visual datasets in GIS, attributes had to be edited, managed, and cataloged in Microsoft Excel.

To characterize the seafloor, a numerical classification scheme modeled after that of Wanless et al. (2006) was created. The scheme is based on observations of the underwater video footage and still photographs. During the process of classifying the seafloor, the dive logbooks that contain geologic notes recorded by the 2002 scientific crew were referred to often. These notes proved to be invaluable because they also provided insights into the discussions that were ongoing during the dives.

For each data point, I associated each surface type with a number and recorded this on a spreadsheet in three columns. One column was assigned for the major or most interesting surface geology and the second and third described minor surface geology, if there were any. Additionally, the amount of sediment cover (%) was estimated. Overall, approximately 6,000 data points were classified to characterize the seafloor.

The logbooks also noted when Jason encountered navigational problems, which occurred mostly upon landing on the bottom. These problems in navigation became apparent when the data points were plotted in GIS. Because of this, I also plotted the ship's coordinates recorded in the logbooks to see if positional errors were significant.

CHAPTER 3. RESULTS

3.1. Overview of Mauna Loa's Submarine SWRZ

The boundary between the Western and Eastern flanks of the SWRZ is defined here by the top of the steep (>20° and in places >30º; Figs. 13) west-facing submarine Kahuku Pali (Fig. 14). Approximately 20 km from the shoreline, at ~2,500 m.b.s.l, the pali dies out and becomes a broad ridge. Beyond this point the boundary between the Western and Eastern flanks is defined by morphologic differences and/or similarities visible in bathymetry and backscatter (Figs. 13-16).

Analyzing morphology and surface textures as they are depicted in bathymetric contours, slope, aspect, shaded-relief, and backscatter datasets helped to establish regions and sub-regions within the Western and Eastern flanks. Generally, these regions and sub-regions exhibit distinct characteristics and occasionally their margins are distinct features such as scarps or shallow valleys. ROV dive observations, where available, provided some ground-truth for the different types of surfaces within regions and sub-regions (Figs. 1, 6, 13-16). In total, five regions (W1-W5) on the Western flank and three (E1-E3) on the Eastern flank were categorized and below they are described in detail (Fig. 6).

3.1.1. Western Flank

The Western flank was divided into five regions (W1-W5; Fig. 6). Region W1 is the submarine Kahuku Pali (e.g., Garcia et al., 1995). West of the submarine Kahuku Pali, from the coastline and seaward, are regions W2 and W3. In this thesis, region W3 is

additionally referred to as the Kahuku Gap. Regions W4 and W5 together make up the east- and west-facing slopes of the West-flank block that lies west of the Kahuku Gap.

3.1.1.1. Region W1 - Submarine Kahuku Pali

The prominent west-facing submarine Kahuku Pali (W1) is an extension of the subaerial Kahuku Pali (Figs. 1, 6, 13-16, 18). The submarine Kahuku Pali is ~1-3 km wide (E-W) by ~22 km long (N-S) and from the coastline, it extends southward to ~2,500 m.b.s.l. The SW coastline partially bounds its NE margin, but mostly its upper margin is the top of the submarine pali. It is bounded to the E, from shallow to deep, by the Eastern flank's regions E1, E2, and E3. Its W margin, from shallow to deep, is bounded in parts by region W2 (to the NW), the Kahuku Gap (W3; to the W), and again by the Eastern flank's region E3, which wraps around to the SW. The pali's SW margin with region E3 is defined by changes in steepness (Figs. 13) and backscatter values (i.e., region E3 has weaker intensities; Fig. 16).

The height of the pali is a few tens of meters near the coastline and as much as 2 km offshore (e.g., Fornari et al., 1979; Garcia et al., 1995). Much of the pali is characterized by narrow ridges and valleys that are oblique or perpendicular to the pali's face. Spacing between the ridges varies from a few tens of meters to a few kilometers, and they are a few tens of meters to a few kilometers in length.

Medium to high backscatter intensities imply that the pali's surface as a whole is rough (Fig. 16). Possibly, this brightness may be affected by the pali's orientation. There are pronounced streaking patterns that correlate with the ridges and valleys

described above. These streaks roughly trend E-W and are composed of alternating low-medium backscatter areas and medium-high backscatter areas.

For the pali ROV data for three dive sites (J-16, -19, -20) located ~10-14 km south of Ka Lae were examined (Fig. 1). These dives traversed the pali in an easterly direction, which is approximately perpendicular to its strike. Observations are presented below, starting with dive J-16 (the deepest) and ending with dive J-20 (the shallowest).

Dive J-16 began at the base of the pali at ~2,400 m.b.s.l and continued upward to ~1,950 m.b.s.l. Between these depths the geology varied from complete sediment cover to lava flows and dikes. From ~2,400 m.b.s.l to ~2,340 m.b.s.l, the surface had >75% sediment cover and sparse rock fragments. From ~2,340 m.b.s.l to ~2,240 m.b.s.l, we noted talus and rough textured outcrops, and sediment cover that range from 25-100%. The lava flows at these depths displays textures that are fluidal (i.e., a draping flow) to jagged and fragmented (i.e. resembling subaerial ‘a‘ā flows). The surface between ~2,240 m.b.s.l and ~2,100 m.b.s.l is mantled by talus and patches of dark sediment. Above ~2,100 m.b.s.l, outcrops protrude through the sediment cover and these lava flows display a knobby surface texture. The ROV came across more of these knobby textured lava flows and several near vertical walls between ~2,090 m.b.s.l and ~1,980 m.b.s.l. Some walls expose pillow lavas, some expose columnar jointed dikes and others have textures that do not resemble pillows or dikes (autobrecciated?). Talus is common at the bases and tops of walls. At ~2,000 m.b.s.l there is a thick unconsolidated sediment outcrop that appeared to be layered and crumbly. The upper part of the traverse, from ~1,980 m.b.s.l to ~1,950 m.b.s.l, shows more talus and patches of dark sediment.

Dive J-19 is less than 60 m south of J-16, starting at ~2,220 m.b.s.l and ending at ~1,350 m.b.s.l (Fig. 1). In general, dive J-19 encountered similar geology as J-16. In dive J-19 dive we observed layered unconsolidated sediment at ~2,120 m.b.s.l. Between ~2,120 m.b.s.l and ~2,000 m.b.s.l the data coverage is sparse due to low visibility. Above ~2,000 m.b.s.l and to ~1,970 m.b.s.l, dive J-19 came across rock fragments, a rugged-surfaced lava flow overlain by unconsolidated sediment, and a wall cross-cut by a dike. In water shallower than 1,970 m.b.s.l and continuing to ~1,740 m.b.s.l the surface consists of blocky fragmented pillows, pillow walls, dikes, hyaloclastite deposits, and talus. The dominant geology between ~1,740 m.b.s.l and ~1,370 m.b.s.l is fragmented pillows and talus. An exception is a near-vertical wall made up of blocky fragmented pillows at ~ 1,370 m.b.s.l.

Dive J-20 was ~200 m NE of dive J-19, starting at ~1,380 m.b.s.l and ending at the top of the pali at ~730 m.b.s.l (Fig. 1). Fragmented pillows, near-vertical pillow walls and dikes were frequently encountered. The bases and tops of pillow walls and dikes are usually mantled by talus and dark sediment patches. On the shallower part of the pali, starting at ~760 m.b.s.l to ~750 m.b.s.l, the surface is predominantly talus, and above ~750 m.b.s.l there is 75-100 % sediment cover with ripples.

3.1.1.2. Region W2

Region W2 runs just offshore of, and parallel to, Mauna Loa's SW coastline, from the NW end of the submarine Kahuku Pali (W1) to the NW corner of the map area, near Kauna Point (Figs. 6, 13-16, 18). Its lower margin is the Kahuku Gap (W3) and its SE margin is the submarine Kahuku Pali (W1). The region is ~2-4 km wide by ~21 km long

and mainly features moderately-steep to steep seaward facing slopes from sea level to ~900-1,200 m.b.s.l.

The irregular margin between W2 and the floor of the Kahuku Gap (W3) is defined by a break in slope (from >25° to <5º; Figs. 13), a change in shaded-relief texture (smooth to rugged; Fig. 15), a change in aspect (slopes generally facing southward to slopes facing multiple directions; Fig. 14), and a change in backscatter (i.e., streaky to mottled patterns; Fig. 16). The margin between W2 and the submarine Kahuku Pali (W1) is similarly defined. Aspect (Fig. 14) and slope data (Figs. 13), for example, show that smooth southward facing slopes of W2 meet rugged westward facing slopes of the pali (W1).

Common on the shallower slopes of W2 are a few steep (can be >25°; Figs. 12, 13, 15, 18) bumpy (knobby) features. In bathymetry these features appear to stand above the surrounding smooth slopes, and in backscatter they tend to be bright (Fig. 16).

Elsewhere, the slopes of region W2 are smoother (Figs. 13b, 15). Slopes are typically >10º (Figs. 13). The alternating streaks of low backscatter areas and medium-high backscatter areas, which are oriented perpendicular to depth contours, areas suggest finer-grained and coarser-grained materials, respectively (Fig. 16). These streaks trend NE-SW and can be as much as a few kilometers in length. We have no dive data for region W2.

3.1.1.3. Region W3 - Kahuku Gap

The Kahuku Gap (W3) is centrally located within the Western flank (Figs. 6, 13-16). It is enclosed by the submarine Kahuku Pali (W1; to the E), regionW2 (to the N),

and the West-flank block (W4 and W5; to the W), extending from depths of ~900-1,200 m to ~4,800 m. Overall the Kahuku Gap is widest at its N, narrowest (~8 km) in its middle, about 20 km from the coastline, and widens again in the S (up to ~20 km parallel to the SW coastline).

The Kahuku gap's northern and shallower half is characterized by four relatively gradual-sloped and moderately smooth steps that are separated by steep margins of variable heights (as much as several hundred meters). In contrast, the gap's southern and deeper half is characterized by irregular slopes marked by a number of concave-seaward scarps.

Landward, the gap shares its boundary with W2 that is defined by distinct changes that are described in the section about W2 above. The gap's SE boundary with the Eastern flank's region E3 is also defined by changes in slope (Figs. 13), shaded-relief data (Fig. 15), aspect (e.g., west dipping; Fig. 14), and backscatter intensity (e.g., stronger for the gap's floor; Fig. 16). Its SW margin is the edge of the study area.

The four broad steps that form the northern and shallower half of the floor of the Kahuku Gap have depths averaging ~1,300 m (step A), ~1,800 m (step B), ~2,400 m (step C), and ~2,600 m (step D) along profile A-A` (Figs. 6, 17). Step A starts at the base of region W2 along a boundary that varies from ~900 m.b.s.l to ~1,200 m.b.s.l. The step is ~20 km long parallel to the coastline and ~1-6 km wide perpendicular to the coastline. Its seaward boundary with step B is concave-seaward and is defined primarily by changes in slope (Figs. 13), ruggedness (Fig. 15) and in places, by backscatter signatures (Fig. 16). This boundary is shallower to the W (~1,300 m) and deeper to the E (~1,800 m).

Despite having slopes that are generally <5º, step A is somewhat bumpy (Figs. 12, 13, 15-16, 18). Some of these bumpy areas correspond with well-defined cone-shaped hills clustered on its western half whereas other bumpy surfaces appear to be associated with broad low-relief areas. Both bumpy areas have backscatter intensities that are medium to high (Figs. 12, 13, 15-16, 18).

Three broad low-relief bumpy areas with high backscatter located on the western half were mapped (i.e., bright sharp margins; Figs. 12, 13, 15-16, 18). Two can be traced back to constructional features (cones and/or pillow mounds?) with heights as much as 200 meters that are clustered together less than 5 km from the coastline (Figs. 12, 18). These cones and/or pillow mounds have similar backscatter values, suggesting that the two broad low-relief bumpy areas and the cones and/or pillow mounds may be linked. The third broad low-relief area is located next to region W4 (Figs. 12, 13, 15-16, 18). This area overall is brighter and more extensive than the two mentioned above and appears to continue downslope across step B, giving it a maximum length of slightly less than 10 km (Figs. 12 and 16). It is not known if this bumpy, bright, and low-relief area is also related to the cluster of cones and/or pillow mounds mentioned above that sits less than 5 kilometers from the coastline.

Centered in the middle of step A is another bumpy low-relief area. Backscatter is medium and the area appears less bright than those observed on western half of step A. Within this area I also observed places of high backscatter that are concentrated in linear patterns. I assumed that these are backscatter artifacts. Moreover, it appears that part of the bumpy area corresponds with at least one well-defined cone-shaped hill (base slightly >500 m) that is distinct in slope (Figs. 13) and shaded-relief (Fig. 15) images. The

relationship regarding their locations and similar backscatter intensities suggests that these features may be related.

At the East end of step A, near the submarine Kahuku Pali (W1) I identified two additional medium-high backscatter areas (Fig. 16) with bumpy surfaces (Fig. 15). They are 2-3 km in length and as much as 1.5 km in width (Figs. 18). Unlike the bright-backscatter areas in the western and middle portions of step A, no obvious well-defined cone-shaped hills are nearby.

Step B, from the base of step A's steep seaward front (~1,300-1,800 m.b.s.l). Its seaward boundary with step C is defined by changes in slope (Figs. 13), elevation (Fig. 15), and roughness (Fig. 16). This boundary is more pronounced closer to the east (at 2,400 m) than to the west (at 1,800 m). Step B's seaward front is roughly concave-seaward.

On step B there are no cone-shaped hills such as those on step A. However, slope data show that the surface is uneven (Figs. 12-13). Even so step B is mostly smooth in shaded-relief data (Fig. 15) and generally dips ~5° southward (Figs. 13-14). Areas that appear bumpy sit at the base of step A (the W end) and region W4 (the N end) and are also associated with step B's seaward facing scarps (especially near the E end; Figs. 12, 18). These bumpier surfaces tend to have stronger backscatter values than the surrounding smooth seafloor (Fig. 16). The broad low-relief areas that abut W4 and step A are distinctively brighter than the seaward facing scarps. As noted above, I consider this area to be the continuation of step A's broad bright low-relief area located directly above it.

In the middle of step B is a low-relief area (~1°) that is smooth in shaded-relief (Figs. 18), yet unusually bright in backscatter image (Fig. 16). Its high backscatter intensities are in sharp contrast to the surrounding seafloor's low backscatter values (Figs. 12c, 16). The area stretches seaward >5 km and at its widest is ~1.5 km (Figs. 18).

Step C extends from the base of step B seaward to ~2,580-2,700 m. This step is mostly smooth with no cone-shaped hills nor distinct broad low-relief areas of high backscatter (Figs. 16, 18). The only areas that appear brighter than the surrounding seafloor correspond with step C's convex-seaward facing scarp. The height of the scarp can be as much as 200 m.

Step D starts at the base of step C at ~2,580 m and extends to 2,700-2,720 m. No remarkable features are identified in step D. It has gradual, essentially featureless slopes with mostly low backscatter (Figs. 13, 16, 18).

Seaward of step D, from ~2,660-2,720 m.b.s.l to ~4,800 m.b.s.l, is the Kahuku Gap's (W3) southern and deeper half. It is characterized by multiple concave-seaward scarps and irregular lumps. Scarps can be as much as ~700 m in height and in places steeper than 30° (Figs. 13). The more prominent scarp belongs to a well-defined amphitheater located at the base of region W5 and the downslope edges of steps B and C (Figs. 13, 18). Associated with this amphitheater is an elongate chute that continues >20 km S (primarily outside of the study area). The chute at its narrowest is <2.5 km wide and at its terminus, between the Dana and ʻĀpuʻupuʻu Seamounts, is a field (~20 km across) of small sized hummocks (~1 km or less across). To the south of the amphitheater are smaller arcuate scarps. Most of these are concave to the southwest (Fig. 14) and in places have scalloped outlines (Figs. 13).

There are a lot of backscatter artifacts in this area, making it difficult to interpret reliable backscatter intensities. For example, the slopes that are near the south end of the SWRZ and the ʻĀpuʻupuʻu Seamount have unusually strong backscatter signatures that do not agree with bathymetry or dive data observations. Elsewhere, despite visible artifacts, backscatter values vary from low to high, but overall intensities are medium to high. Steep scarps are typically bright, indicating low sediment cover and/or rough surfaces.

3.1.1.4. Region W4 - East-facing scarp of the West-flank Block

About 10 km S of Pōhue Bay is a large submarine block and I defined region W4 as its prominent east-facing scarp (Figs. 6, 13-16, 18). Like the submarine Kahuku Pali (W1), W4 is steep (can be >20°) and rugged. It is ~1-2 km wide (NE-SW) by ~17 km long (NW-SE). Both its upper (W) and lower (E) margins start at ~1,240 m.b.s.l and end at ~2,450 m.b.s.l. W4 is bounded by W5 to the W (the block's west-facing slope), and by the Kahuku Gap (W3) to the E.

Region W4's lower E margin with the floor of the Kahuku Gap (W3) is an obvious break in slope, from ~15-20° and rugged (W4) to <5° and smooth (W3). W4's margin with W5 is defined mainly by slope and aspect (Figs. 13-14). Depth differences between W4's upper and lower margins are as much as 800 m. Like the Kahuku Pali (W1), W4 is steep, rugged, and features narrow ridges and valleys. W4's ridges and valleys are spaced several hundred of meters apart and are a few tens of meters to several kilometers in length. Towards the southern end they are less pronounced.

Backscatter intensity overall is strong for region W4 (Fig. 16). Here, medium to medium-high backscatter values indicate rough surfaces. Streaking patterns are recognized, but these mainly occur at the northern end of the region where ridges are noticeable. Streaks of alternating low-medium and medium-high backscatter areas suggest variable surface roughness (e.g., fine- versus coarse-grained deposits). The streaks generally trend W-E, parallel to the strikes of the ridges and valleys, and some continue downslope to the base of the region.

3.1.1.5. Region W5 - West-facing slope of the West-flank Block

Region W5, like W4, is part of the large submarine block located ~10 km S of Pōhue Bay (Figs. 6, 13-16, 18). W5 defines the West-flank block's mostly west-facing slopes. Within our map area W5 shallows to ~600 m.b.s.l and deepens to ~3,310 m.b.s.l. The region is roughly triangular in shape, with the tip located at ~1,240 m.b.s.l. Towards its S end W5 widens to ~7 km (E-W). These dimensions are partly artifacts of the study area's edge.

The S margin is convex southward and is bounded by the southern and deeper half of the Kahuku Gap (W3). This margin is defined where W5's steeper (>15°) rugged slopes transition to the floor of Kahuku Gap's (W3) less steep (<15°) and somewhat less rugged slopes (Figs. 13). The E margin of W5 is the top of the W4 scarp.

Slope and aspect show that region W5 is characterized mainly by slopes dipping southwestward approximately at angles of <15º. The exceptions are slopes at the N and S end which tend to slope >15º westward and southward, respectively (Figs. 13-14). W5 is distinctively smooth, but also has areas where slopes are bumpy (Fig. 15).

Backscatter values vary from low to medium-high, with low values common on gradual slopes and medium to high values are common for the rest of W5 (Fig. 16). This observation indicates that W5's roughness varies. It is also important to note though that artifacts are present in backscatter data in this area.

3.1.2. Eastern Flank

The Eastern flank is comprised of three regions which are, from shallow to deep E1, E2, and E3. Part of region E3 is an inlier within E2. Region E3's bathymetry is complex, thus it has been divided into sub-regions (E3a to E3o; Fig. 6; Appendix A).

3.1.2.1. Region E1

Region E1 runs just offshore of, and parallel to, Mauna Loa's SE coastline. It slopes gently seaward from shore to ~100-200 m.b.s.l, and is relatively smooth (Figs. 6, 13-16, 18). Specifically, E1 is elongate in a SW-NE direction, and is ~3-7 km wide by ~17 km long. The submarine Kahuku Pali (W1) defines its western edge. Its seaward margin (SW-SE) is defined by an abrupt change in slope from <5° to >20° (Figs. 13). At the SW end of E1, this change in slope occurs at ~160-200 m.b.s.l, and it shallows gradually to ~100 m.b.s.l at the NE end. E1 is widest (~7 km) at its SW end, and narrows to ~3 km at its NE end. Almost all of E1 slopes <5° to the S-SE (Figs. 13-14) and it is comparable to, and essentially a continuation of, the adjacent subaerial Mauna Loa slopes.

In shaded-relief data, E1is distinctively smooth (Fig. 15). Backscatter data, although not available for all of E1, exhibits predominantly low values (Fig. 16). An

exception is the SW part of E1, near the submarine Kahuku Pali (W1). Here, low to medium backscatter values (in patches with areas of ~1 km^2 and greater) are juxtaposed together, produce a speckled and in some areas a marbled pattern.

3.1.2.2 Region E2

Region E2 is located immediately downslope of region E1 (Figs. 6, 13-16, 18). It includes steep rugged terrain seaward of the slope break that marks E1's seaward edge. This terrain extends from ~100-200 m.b.s.l to ~1,200 m.b.s.l, and is characterized by narrow valleys and ridges. In deeper water (>1,200 m.b.s.l to ~4,100 m.b.s.l) slopes are less rugged and less steep. Region E2's landward margin extends in a SW-NE direction (>20 km long) and from the SW to the NE corner of the mapped area it is bounded in parts by the submarine Kahuku Pali (W1), the seaward margin of E1 (i.e. the slope break), and Mauna Loa's SE coastline. Part of region E3 protrudes out of the E part of E2. It is an irregularly-shaped and uneven terrain that stands tens to hundreds of meters above the surrounding seafloor. E2 is narrowest at its W end (<1 km wide) and widest at its E end (perpendicular to contours it can measure up to ~13 km).

The slopes stretching from ~100-200 m.b.s.l to ~1,200 m.b.s.l vary in steepness and in places can be >20°. Bathymetric contours, shaded-relief, and aspect images reveal that between these depths, E2's steep SE-facing slopes are cut by NW-SE trending valleys that extend seaward from just below the slope break (Figs. 13-15). These ridges and valleys give the upper part of E2 its rugged morphology (Figs. 13, 15). The floors of the valleys commonly exhibit low backscatter values, whereas backscatter values for ridges tend to be medium-high (Fig. 16). From the mouths of these valleys, low

backscatter streaks continue downslope to the SE as far as a few kilometers. The overall effect is a streaked pattern of rough and smooth terrain. Valleys are spaced a few tens of meters to a few kilometers apart, and become faint ~1-3 km downslope from the slope break. At their heads, the valleys are several tens to hundreds of meters deep, and their floors are a few tens to hundreds of meters wide.

Below ~1,200 m.b.s.l, region E2 slopes decrease to <10° at ~4,100 m.b.s.l. Compared to the upper part of E2, this deeper part is smoother, as indicated by bathymetry (Fig. 15). Backscatter data indicate variable surface roughness (Fig. 16). The combination of low, medium, and high backscatter values results in a densely peppered pattern that is generally bright. This pattern shows that for depths >1,200 m E2's surface roughness is variable, but overall rough.

3.1.2.3. Region E3

Region E3 is located downslope from E2 (Figs. 6, 13-16, 18). It starts on the west from the top of the submarine Kahuku Pali (W3) and extends E and S from ~420 to ~4150 m.b.s.l. E3 is elongate in a NE-SW direction, and is ~30 km long and ~17 km wide. It is characterized by gradual to steep slopes and encompasses many positive (e.g., cone-shaped hills and flat-topped constructs) and negative (e.g., valleys, scarps, depressions) bathymetric features. Abundant constructional features within the region give E3 its distinct rugged surface.

The margin between E3 and E2 occurs where E2's relatively smooth slopes meet E3's more rugged slopes. This margin coincides with a change from generally southward facing slopes to more eastward facing slopes (Fig. 14). The margin between regions E3

and the submarine Kahuku Pali (W1) is an abrupt break in slope (Figs. 13). Less obvious is region E3's W-SW margin with the Kahuku Gap (W3). This margin is defined by changes in slope (Figs. 13), shaded-relief (Fig. 15), aspect (e.g., west dipping; Fig. 14), and backscatter values (i.e., stronger intensities for the gap's floor; Fig. 16). Common along this margin are small steep scarps and this distal part of the Eastern flank lies west of the bathymetric high.

Region E3 is further divided into sub-regions (E3a-E3o). For general descriptions, refer to Appendix A.

Region E3 was surveyed in four ROV dives (J-20, -23, -24, -25; Fig. 1) within a ~10 km wide (E-W) strip centered along the flank's bathymetric high. The shallowest dive was J-20 at less than 10 km from Ka Lae and the rest were ~24-35 km from the coastline. J-20,-24, and -25 traversed in a NE direction whereas J-23 ascended in NW direction.

Approximately 1.5 km of dive J-20 traversed the shallow N end of region E3 (Fig. 1). Specifically, starting from the top edge of the submarine Kahuku Pali (W1) at ~800 m.b.s.l and ending at the top of a mound at ~480 m.b.s.l. At ~690 m.b.s.l, slopes are gradual and dead coral fragments and ripples can be observed. The main surface type between the slope break and ~680 m.b.s.l is sediment cover (75-100%). From ~680 m.b.s.l to ~660 m.b.s.l, the surface, which is bright in backscatter, consists mostly of rock fragments and pillow lavas. Sediment cover is <25 % (sometimes rippled) and the sediments tend to concentrate at low points between pillows and rock fragments. Dark patches of sediment are observed, as well as fauna. Rock fragments continue to be the dominant surface type between ~660 m.b.s.l and ~650 m.b.s.l; however, sediment cover

varies from 25-100 %. Between ~650 m.b.s.l and ~630 m.b.s.l., sediment cover is ~75-100 % and rock fragments are sparse. In places, sand and rock fragments create a mottled surface. Loose sediment, dead coral, rock fragments, and occasional pillows are common between ~630 m.b.s.l and ~480 m.b.s.l. An exception to this is a dike at ~530-550 m.b.s.l and talus at its base and top. Near the end of the dive a mantling flow with fluid textures (e.g., ropey) is observed at ~520 m.b.s.l. The dive ended at the top of a mound (~490 m.b.s.l). Here dead corals and a sheet-like lava flow were noted.

Dive J-23 began at the base of a scarp at ~4,000 m.b.s.l and ended at the top of a constructional feature (~500 m diameter) at ~3,050 m.b.s.l (Fig. 1). Sediment cover for this depth interval ranged between 50-100%. The common surface cover seen along this dive is pillows (e.g., intact, broken, bulbous, and/or elongated) and on steep slopes they occur as mantling flows. Two dikes were identified at ~4,018 m.b.s.l and ~3,680 m.b.s.l and one sheet-like flow overlying pillows occurred at ~3,910 m.b.s.l. In close proximity to these dikes and the sheet-like flow are draped unconsolidated sediments (some layered). Small localized debris flows were observed at ~3,850-3,860 m.b.s.l, ~3,810 m.b.s.l, and ~3,635 m.b.s.l. Draped unconsolidated sediment outcrops at ~3,540 m.b.s.l and ~3,510 m.b.s.l are distinctly layered. Lobate pillows are frequent near the top of the constructional feature and at the top (~3,080 m.b.s.l) subtle ripples and faint outlines of mini collapse features can be observed.

Dive J-24 surveyed the southwestern tip of the Eastern flank, from approximately 4,000 m.b.s.l to ~3,640 m.b.s.l (Fig. 1). Specifically, this dive ascended steep seaward-facing slopes of a large constructional feature (base ~ 5.5 km across). From its base to ~3,840 m.b.s.l, talus and pillows (broken, intact, elongate, and lobate) were encountered

and sediment cover for this depth interval ranged from 50-100 %. A few small collapse pits were seen on the surfaces of lobate flows. Areas with the least amount of sediment cover (as low as 0-25 %) usually are associated with knobby textured massive outcrops (e.g., brecciated pillows) that crop out at ~3,850 m.b.s.l. and ~3,840 m.b.s.l. Above ~3,840 m.b.s.l to 3,650 m.b.s.l, sediment cover is generally high (75-100%) with sparse rock fragments. Small rock outcrops sometimes protrude through the sediment cover. Only two major outcrops of bulbous, elongate, and/or lobate pillows with partially broken surfaces were crossed at this depth interval where sediment cover is 50-75%. One is at ~ 3,745-3,710 m.b.s.l and the other is at ~3,680 m.b.s.l. Sheet-like flows with a fluidal, ropy surface, however, were encountered at the shallower outcrop. The surface of this outcrop was also indented by several small collapse pits.

Dive J-25 (Fig. 1), from ~3,590 m.b.s.l to ~3,350 m.b.s.l, ascended three mounds. The mounds' steep outer slopes are mostly covered by rubble and pillows (intact and broken, bulbous, bulbous with breadcrust textured surface, and lobate pillows). At a few locations 'a'ā- like flows, flows with slabby surface textures, and localized rubble/talus slopes were noted. Sediment cover for this depth interval varies from 0-25% to 50-75%. For areas with high sediment cover (mainly the tops of mounds), dark sediment patches are common.

Above the mounds J-25 ascended a large constructional feature. Between ~3,350 m.b.s.l and ~3,250 m.b.s.l, J-25 encountered rubble and lava outcrops with knobby surfaces (e.g., breccia topped flow?). In places these knobby outcrops are hard to distinguish from the surrounding surface rubble. From ~3,250 m.b.s.l to ~3,180 m.b.s.l, pillows (e.g., lobate), both intact and broken are the dominant surface rock type. Sparse

corals are observed. From ~3,180 m.b.s.l to ~3,160 m.b.s.l, occasional pillows (e.g., lobate), rubble, and coral were noted as well as dark sediment patches and ripples where sediment cover is high. Continuing to water depths of ~2,960 m.b.s.l, more lone pillows, usually with broken surfaces, were crossed. From ~3,030 m.b.s.l, dive J-25 ascended another constructional feature. Dark and light sediment patches and small rock fragments are seen throughout the dive. Rubble covered slopes between ~2,950 m.b.s.l and ~2,900 m.b.s.l transition into an extensive talus outcrop from ~2,900 m.b.s.l to ~2,870 m.b.s.l. Intact and broken pillows (e.g., elongate and lobate) are immediately above the talus slope. An exception is a dike at ~2,850 m.b.s.l. As the dive ascended the steepest part of the constructional feature, talus was found at the base of truncated pillows at ~2,790 m.b.s.l. From this depth to ~2,730 m.b.s.l, the surface consists of intact pillows, rubble, and coral. More pillows (e.g., lobate and bulbous), rubble, and sparse corals are near the edge and across parts of the feature's top (~2,730 m.b.s.l to <2,700 m.b.s.l). Dikes were encountered at roughly ~2,715-2,720 m.b.s.l and ~2,700 m.b.s.l. The deeper dike crosscuts a pillow outcrop whereas the shallower dike protrudes out of rubble and sediment covered slopes. J-25 continued down the sides of the constructional feature and across the top and sides of another smaller constructional ridge to the north, ending at ~2,730 m.b.s.l. On the ridge the dive encountered outcrops that are knobby with broken surfaces. Sediment cover was highly variable along the J-25 dive track (0-25% to 75-100%).

CHAPTER 4. DISCUSSSION

The geomorphologic features on the Western and Eastern submarine flanks of Mauna Loa's SW rift zone are generated by a combination of constructive and destructive processes. Differences in the types of features and the extent of their coverage help to determine which processes are more dominant. For instance, the Western flank is dominated by features produced by destructive processes (e.g., collapse scars) and its present surface is likely young, whereas the Eastern flank consists primarily of constructional features (e.g., volcanic cones) which may be rather old. Collectively, these observations show that Mauna Loa's submarine SWRZ geologic and tectonic history is complex.

4.1. Western Flank

The Western flank is marked by an erosional morphology; the main feature is termed the Kahuku Gap (W3; Figs. 6, 13-16, 18). The Kahuku Gap is similar in gross morphology to the Kaupō Gap, a prominent erosional feature on the subaerial south flank of Haleakalā volcano (Maui). The floor of Kaupō Gap has been partly re-filled by post-shield volcanism (e.g., Sherrod et al., 2007). Both features have a relatively planar floor that is wider at the upper elevations and narrows downslope. The scarps that bound the Kahuku and Kaupō Gaps are ~600-2,000 m and ~600-1,000 m high respectively.

The Kahuku and Kaupō Gaps are morphologically alike, but have been formed by different erosional processes. The Kaupō Gap is a stream-cut valley and its shape (wider at the head) is due to accelerated erosion of weaker material at the summit of Haleakalā

(e.g., pyroclastics and rocks altered by gas; Macdonald et al., 1983). For the Kahuku Gap, the widely accepted model suggests that the gap was created by gravitational failure(s) (e.g., landslides; Lipman 1980).

We propose that the Kahuku Gap was formed in four stages of mass-wasting with these stages contributing to the East Ka Lae landslide (Fig. 19). We base our hypothesis on observations of distinct surface patterns in bathymetry and crosscutting relationships within the gap's shallower northern and deeper southern halves and nearby regions (Figs. 6, 13-19). The shallower northern half consists of relatively flat broad steps A, B, C, and D which have average depths of ~1,300, ~1,800, ~2,400, and ~2,600 m, respectively along profile A-A` (Figs. 6, 17). Below step D, broad and relatively planar steps are absent. Instead, the gap's deeper southern half is carved by steep concave-seaward scarps. The most prominent scarp is the ~700 m deep horseshoe-shaped amphitheater that is located at the base of the West-flank block (W5). This scarp cuts into the west sides of the two deepest broad steps, C and D (Figs. 18, 19). Along the Eastern flank's south-southwest margin and ʻĀpuʻupuʻu Seamount's northwest margin, the concave-seaward scarps are less pronounced, small and discontinuous. Collectively they cut into step D as well as the south-southwestern most portion of the (mostly constructional) Eastern flank (Figs. 18, 19).

We also suggest that during and/or since the formation of the East Ka Lae landslide, volcanic activity and depositional processes resurfaced part of the gap's floor. This idea is supported by the presence of steps (A, B, and perhaps C; Figs. 17-19) and the gap's dominantly smooth character in shaded-relief (Fig. 15) and slope images (Figs. 13). High backscatter signatures on steps A and B (from this study) and documentation of

fresh-looking lava flows by Fornari et al. (1979) and Garcia and Davis (2001), present compelling arguments for relatively young post-gap volcanism (Figs. 12c, 16).

4.1.1. The Kahuku Gap: Stages 1−4

4.1.1.1. Stage 1a-b

We propose that the predominant shape of the Kahuku Gap was created by Stage 1a, which removed most of the material (~300-500 km^3; Appendix B) and was likely catastrophic. Stage 1a produced high standing scarps, including the submarine Kahuku Pali and scarps of the West-flank block. We base our hypothesis that the East Ka Lae landslide involved complete break-up of the failing material, likely in a catastrophic manner, on two arguments. First, we do not observe any large (>2 km) slump blocks from the Kahuku Gap downslope on the ocean floor (Fig. 19). Instead, hummocks on the floor are about one kilometer or less across (Fig. 19). Second, the middle part of the gap is narrower than the upper part (~8 km versus ~20 km respectively). It would not have been possible for intact slump blocks to have moved downslope through the narrow gap (Figs. 18-19).

A catastrophic hypothesis for Stage 1a, however, does not address the presence of flat broad steps A, B, and C that stand tens of meters to a few kilometers above step D at the base of the slide (Figs. 17-19). To explain their origin, we suggest that the gap's floor was in part resurfaced in Stage 1b by volcanic activity and depositional processes (e.g., volcaniclastics from ocean entries and fragmental material derived from steep scarps). Considering the steps' morphology, this resurfacing explanation is consistent with step C's seaward facing scarp (Figs. 16-18). If step C's scarp was formed by mass-wasting,

we would expect it to be concave-seaward shaped as observed, for example, for the scarps within the gap's deeper southern half (Figs. 18-19). Instead step C is convex-seaward, favoring the idea of a constructive origin.

No volcanic cones were observed on steps below step A. This may be due to an artifact of spatial resolution; volcanic features are smaller than what our data can resolve. Wanless et al. (2006) suggested that small vent size (<10 m high) may explain why three of their mapped lava flows in Kealakekua Bay could not be traced back to their source vents, although the flows themselves were clearly visible in their bathymetric and backscatter data. Bathymetry and backscatter data for our study was collected during the same cruise; therefore, for our study area we may similarly not be able to identify present cones due to their small size. As an alternative explanation, it is also plausible that vents are undetectable because subsequent activity has eroded and/or buried them. The lack of vent structures may also be attributed to fissure eruptions. Fornari et al. (1979) documented north-striking fissures, 1-2 m wide and 2-3 m deep on step B.

4.1.1.2. Stage 2

We suggest that Stage 2 caused part of the Eastern flank (sub-region E3l; Figs. 6, 19) to slump on top of step D's east side. Sub-region E3l also appears to bury part of the south end of the submarine Kahuku Pali. We cannot determine the nature of this burying material, and we have considered that it is possible that volcanic activity built these overlying features after step D. This hypothesis would require that the overlying features of sub-region E3l post-date at least the deepest portion of the submarine Kahuku Pali. However, age data relationships from nearby regions do not support a post-Stage 1b

volcanic origin and all of the dated flows are older than the East Ka Lae landslide's estimated maximum age limit of ~120 ka (Jicha et al., 2012; Figs. 18). Furthermore, this age relationship is supported by our dive and backscatter data (Figs. 6, 16). For example, along dives J-23, -24, and -25, the ROV frequently encountered lava outcrops with high sediment cover (50% or greater). Also, the slopes above step D tend to exhibit low backscatter intensities, indicating sub-region E3l has an older age (Fig. 16). Wanless et al. (2006) demonstrated the good correlation between relative ages assigned from sediment cover and backscatter intensities. Since age data are not available for sub-region E3l, these indirect methods provide useful indicators of relative age.

Morphologic observations support the proposal that sub-region E3l slumped during Stage 2. We note that in the bathymetric data, sub-region E3l displays slightly different surface textures than sub-region E3a that is located immediately upslope of it (Figs. 6, 13-16, 18, 19). Slopes interpreted to have undergone slumping appear to be much smoother than constructional slopes (Figs. 6, 13, 15, 18). The slumped sub-region E3l is especially noticeable in a 3-D perspective image (Fig. 19). The constructional features within E3l are less distinct than constructional features elsewhere on the Eastern flank (e.g., E3e and E3m) and in places their scarps are scalloped (Figs. 6, 13). Assessments of these observations, interpretations from dive and backscatter data, and age data support the idea that Stage 2 of the East Ka Lae landslide consisted of slumping of the Eastern flank's distal southwestern margin (Figs. 6, 16, 18, 19).

4.1.1.3. Stage 3

We propose that Stage 3 generated the southernmost concave-seaward scarps that cut into step D, the overlying Eastern flank's sub-region E3l, and the south-southwest tip of the Eastern flank (E3n; Figs. 6, 18, 19). Runout from slope failures could not be distinguished at the base of the scarps, suggesting that Stage 4 eroded and/or buried this evidence.

4.1.1.4. Stage 4

The East Ka Lae landslide was likely the culmination of Stage 4. During this stage a debris avalanche truncated the Kahuku Gap's deepest steps C and D and the lower reaches of stage 3 deposits. The failure produced a ~700 m-deep amphitheater, a debris chute, and a broad field of hummocks (blocks ~1 km and less across) that lie at the base of the SWRZ, Dana Seamount, and ʻĀpuʻupuʻu Seamount (Figs. 6, 13-16, 18, 19). Discontinuous levees were also generated on the sides of the chute (Fig. 19). The distal hummocks are well-preserved with a youthful appearance that is similar to ʻĀlika 2 deposits (Moore and Chadwick, 1995).

4.1.2. Post-Gap Processes

Bathymetric data show no indication that major flank failure(s) have occurred since Stage 4. There is clear evidence though, that eruptive and depositional (e.g., volcaniclastics formed from ocean entries and intact shoreline-crossing flows) processes continued within the Kahuku Gap's shallower northern half after Stage 1b (Figs. 12, 18). Morphology and backscatter data indicate that this area was partially resurfaced by recent

post-gap volcanism (Figs. 12, 16). The rugged and sometimes smooth broad low-relief areas and cone-shaped hills on steps A and B may be lava flow fields and eruptive vents that were emplaced relatively recently (Figs. 12, 16, 18). We infer this from the features' distinct high backscatter signatures that starkly contrast with the surrounding floor, reflecting their youthfulness (Figs. 12, 16). Wanless et al. (2006) had similar conclusions for features in Kealakekua Bay.

Our interpretation of relatively young post-gap volcanism is supported by Pisces V (P5) dives conducted by Fornari et al. (1979; P5-105, -107, -189) and Garcia and Davis (2001; P5-389). These dives crossed parts of mapped lava flow fields on the west end of step A (Figs. 12, 16, 18). Another dive by Fornari et al (1979; P5-107 appears to have crossed the southern tip of the lava flow field mapped in the center of step B (Figs. 12, 16, 18). Fresh-looking intact pillow flows were encountered on all of these dives. Some of the lava flows on steps A and B appear to have traveled at least 5 km from their source vents.

Regions W2 and W5 also have generally smooth slopes in the shaded-relief data, but in backscatter data they have variable surface roughness that is generally bright (Figs. 6, 16, 18). Furthermore, mottled and streaked areas, and streaks that are perpendicular to the coastline in backscatter data are common in these regions (Figs. 6, 16). The smooth slopes in W2's are probably associated with an apron of volcaniclastics and sediment deposits that mantle this area. Similar features are seen by SCUBA divers who surveyed Kīlauea's Ki‘i ocean entry site who observed slope materials ranging in size from fine sand to boulder fragments and suggested that the same type of materials continue downslope to abyssal depths (Sansone and Smith, 2006). In their backscatter imagery,

streaks extended to ~3,000 m.b.s.l, ~15 km offshore (Sansone and Smith, 2006). The smooth nature of region W5 may be due to mantling of volcaniclastics and sediment and perhaps the West-flank block's age.

Not all ocean entries fragment and generate deposits that appear smooth in shaded-relief. For example, on the shallower slopes of W2 there are a few steep and rugged terrains (Figs. 6, 12, 18). These features are likely lava flows that erupted subaerially and remained relatively coherent even after crossing the shoreline. Such flows have been documented in Kealakekua Bay (i.e., the subaerial Waiea flow traveled ~3.5 km offshore; e.g., Trusdell and Lockwood, unpub. data; Wolfe and Morris, 1996; Wanless et al., 2006).

4.2. Eastern Flank

This region appears to be mostly rugged at a scale of tens to hundreds of meters due to abundant constructional features (Figs. 6, 13-16, 18). This morphology is similar to the submarine portions of Hawaiian rift zones (e.g., Lonsdale, 1989; Moore and Chadwick, 1995; Parfitt et al., 2002; D. Smith et al., 2002; J. Smith et al., 2002; Gregg and Smith, 2003; Eakins and Robinson, 2006) as well as non-rift-zone submarine flanks of Kaua'i (e.g., Flinders et al., 2010). Many of the constructional features in the Eastern flank area are distinct, with dimensions similar to those of the flat-topped and steep-sided cones on Hāna and Puna ridges (Appendix A).

Bathymetry and acoustic backscatter imagery show that the Eastern flank has fewer mass-wasting features than the Western Flank. Steep concave-seaward scarps are as much as a few kilometers wide (Fig. 14). Examples include scarps on the upper slopes

of region E3 (Figs. 18). They appear to have formed from localized landslides rather than major flank-wide events. Based on the Eastern flank's rugged morphology and the absence of large-scale collapse features, we conclude that the flank's present surface formed primarily by constructional processes instead of destructive processes.

CHAPTER 5. CONCLUSION

In this study we examined and characterized Mauna Loa's submarine SWRZ and its Western and Eastern flanks in detail. We produced a new geologic map of the area on the basis of observations made from high spatial resolution bathymetry (~30 m), acoustic backscatter, and Jason dive datasets. Our main findings on the differences between the Western and Eastern flanks are as follows:

1) Distinct patterns in bathymetry and backscatter and distribution of features (e.g., cones and scarps) indicate different roles of constructive and destructive processes on the Western and Eastern flanks. Specifically, the Western flank is dominated by a large bathymetrically negative feature (the Kahuku gap), that has been only partially infilled by younger lavas and sediments. The Eastern flank, on the other hand, is dominated by constructional features such as pillow mounds and volcanic cones represented by hummocky/bumpy terrain in the bathymetry, all of which appear to be quite old.

2) The Western flank's morphology was generated by the East Ka Lae landslide. We recognize that at least four stages of mass-wasting contributed to this landslide. Following mass-wasting, the floor of the Kahuku Gap was partially resurfaced by volcanic activity and depositional processes (e.g., volcaniclastics from ocean entries and fragmental material derived from steep scarps). Features that appear youthful within the gap were also examined and their presence suggests that volcanic activity in the area is likely ongoing. Furthermore, evidence of fairly recent shoreline-crossing flows is

apparent in the nearshore region, W2. From these observations we infer that the present surfaces of the gap and W2 are likely young.

3) These different morphologies roughly mimic the pattern observed on the subaerial SWRZ, and support the hypothesis of Lipman et al. (1990), in which the West flank of Mauna Loa is in a state of recovery from one or more large West-directed mass-wasting events. The East flank, on the other hand, has mostly been protected from resurfacing by topography, and therefore presents an old appearance.

Table 1. Submarine landslides on the western and southern flanks of Mauna Loa volcano.

Name	Type	Estimated Age (ka)	Source*
ʻĀlika 1	debris aval.	200-250	McMurtry et al., 1999
ʻĀlika 2	debris aval.	100-125	Lipman et al., 1988; Moore et al., 1994; McMurtry et al., 1999; McMurtry et al., 2004
East Ka Lae	debris aval.	possibly <30, <60	Moore et al., 1990; Garcia et al., 1995
East Ka Lae	debris aval.	max ~120	Jicha et al., 2012
West Ka Lae	debris aval.	post-ʻĀlika	Moore et al., 1995
North Kona	slumps	>115-130, <300	Moore and Clague, 1992; Moore and Chadwick, 1995; Lipman and Coombs, 2006
South Kona	debris aval. and slumps	>10, <250	Moore et al., 1987; Moore and Clague, 1992; Moore et al., 1995; McMurtry et al., 1999; Moore and Chadwick, 1995; Morgan and Clague, 2003; Lipman et al., 2003; Yokose and Lipman, 2004; McMurtry et al., 2004

*Primary source and selected studies that focused on landslides listed.

FIGURE CAPTIONS

Figure 1. Shaded-relief image of Hawai‘i and the surrounding seafloor (after Wanless et al., 2006). Historical lava flows, ground cracks, and fissure vents taken from Trusdell et al. (2006). Jason dive locations are labeled J-16, -19, -20, -23, -24, and -25. Map is projected in North American Datum of 1983, UTM Zone 5.

Figure 2. Aerial view of Nīnole Hills from the southwest (Lockwood and Lipman, 1987).

Figure 3. Kealakekua Bay with Kealakekua Pali to the east of the bay (Macdonald et al., 1983).

Figures 4a-b. Ka Lae area with the Kahuku Pali and historical lava flows labeled. a) taken by U.S. Navy in 1954 b) from Macdonald et al. (1983)

Figure 5. Geologic map of Hawai‘i and surrounding seafloor by Moore and Chadwick (1995).

Figure 6. The Western and Eastern flanks of Mauna Loa’s submarine SWRZ divided into regions and sub-regions. Figures 7-12 outlined in boxes. Location of profile A-A` is also shown. Shaded-relief is illuminated from the south.

Figure 7. Bathymetric contours of cone 5 (See Appendix A).

Figures 8a-b. Shaded-relief images of cone 5 with contours superimposed. a) Illumination from the southeast (arrow) b) Illumination from the southwest (arrow)

Figures 9a-d. Slope maps of cone 5 and the study area. a) A classified slope map with warm colors representing steep slopes and cool colors representing gradual slopes. b) Slope map with values stretched along a gray scale. Steep slopes are dark gray and gradual slopes are light gray. c) Classified slope map of the study area. Slope values categorized into 8 classes. d) Classified slope map showing only the last three classes.

Figure 10. Aspect map of cone 5. In general, slopes facing northward and eastward are displayed with warm colors whereas slopes facing southward and westward are displayed with cool colors.

Figure 11. Backscatter image of cone 5. Areas that appear bright indicate rough surfaces. Dark areas suggest relatively smooth surfaces.

Figures 12a-c. Slope and backscatter maps for selected features located on the floor of the Kahuku Gap's shallower northern half (i.e., step A and B in W3).

Figures 13a-b. Slope maps of the study area with boundaries of regions superimposed. a) Classified b) Stretched gray scale

Figure 14. Aspect map of study area with boundaries of regions superimposed.

Figure 15. Bathymetric map of the study area that is underlain with shaded-relief. Region boundaries are superimposed. Illumination is from the north.

Figure 16. Backscatter image of the study area with boundaries of regions superimposed. Areas of relatively high acoustic reflectivity (i.e., low sediment cover) are bright and areas of low acoustic reflectivity are dark (i.e., high sediment cover).

Figure 17. Profile A-A` of the broad steps A, B, C, and D of the Kahuku Gap. Profile location is shown in Figure 6.

Figures 18a-b. Geologic map of Mauna Loa's submarine SWRZ underlain with shaded-relief. Illumination from the south. Expanded explanation of the geologic map shown in Figure 18b.

Figure 19. Stages 1-4 of the East Ka Lae landslide generalized.

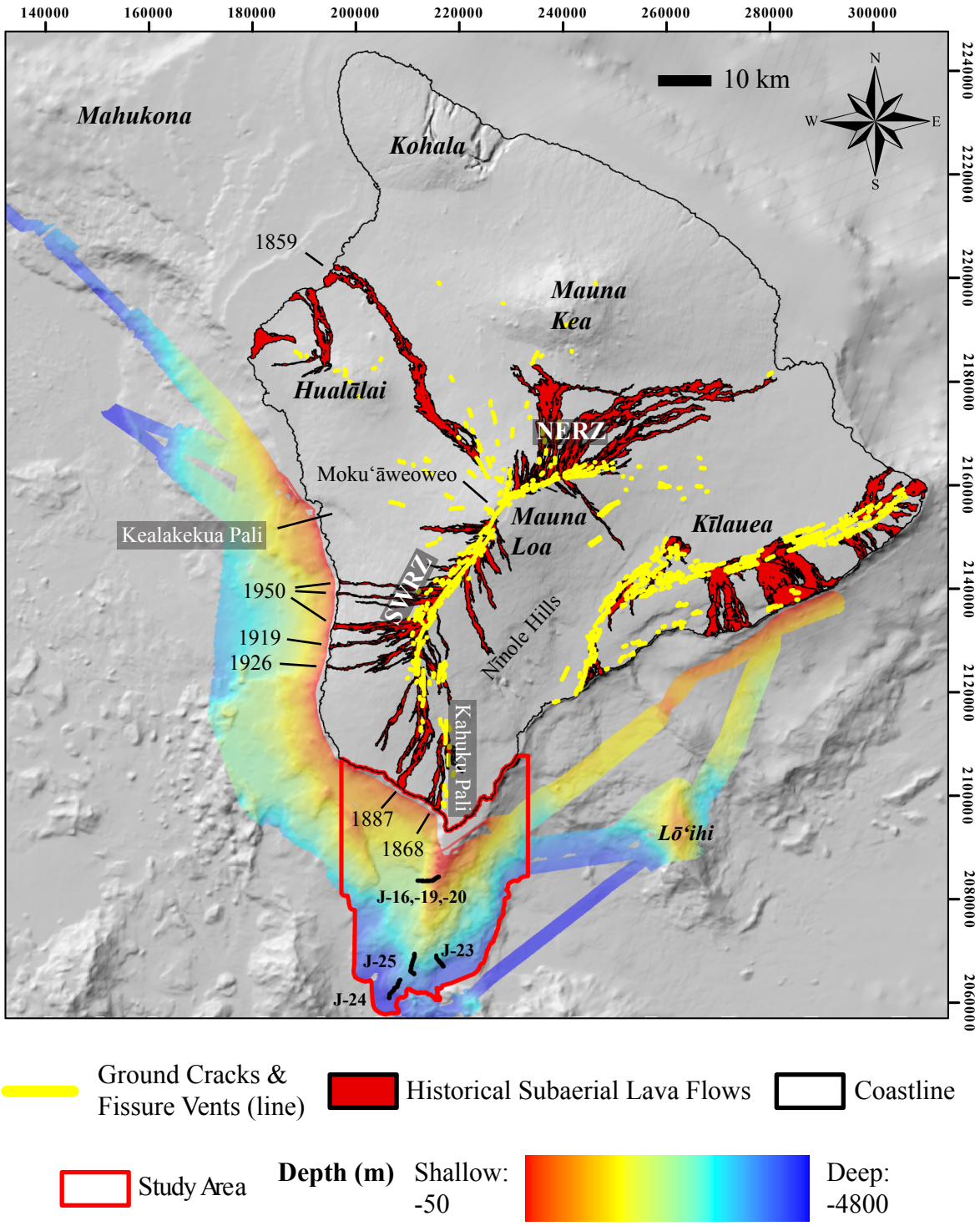
140000
160000
180000
200000
220000
240000
260000
280000
300000
2240000
2220000
2200000
2180000
2160000
2140000
2120000
2100000
2080000
2060000
10 km
N
W
E
S
Mahukona
Kohala
1859
Mauna Kea
Hualālai
NERZ
Moku'āweoweo
Mauna Loa
Kīlauea
Kealakekua Pali
SWRZ
1950
1919
1926
Nīnole Hills
Kahuku Pali
1887
1868
Lō'ihi
J-16,-19,-20
J-25
J-23
J-24
Ground Cracks & Fissure Vents (line)
Historical Subaerial Lava Flows
Coastline
Study Area
Depth (m)
Shallow: -50
Deep: -4800

Figure 1.

Figure 2.

Figure 3.

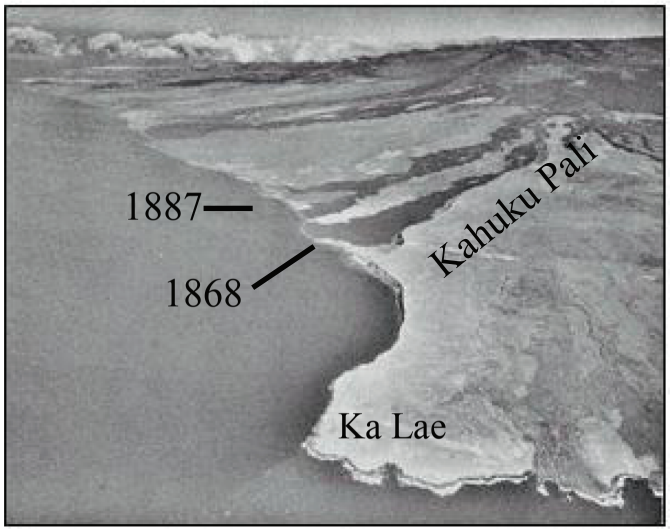

Figure 4a.

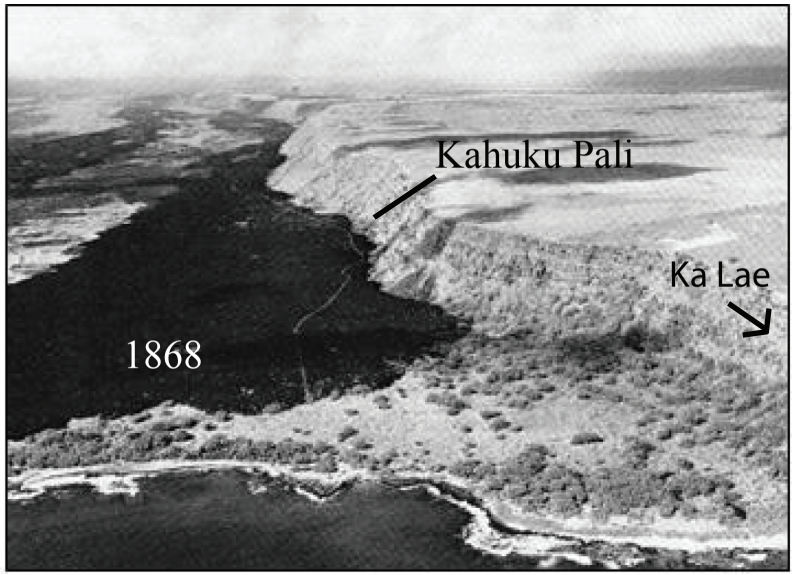

Figure 4b.

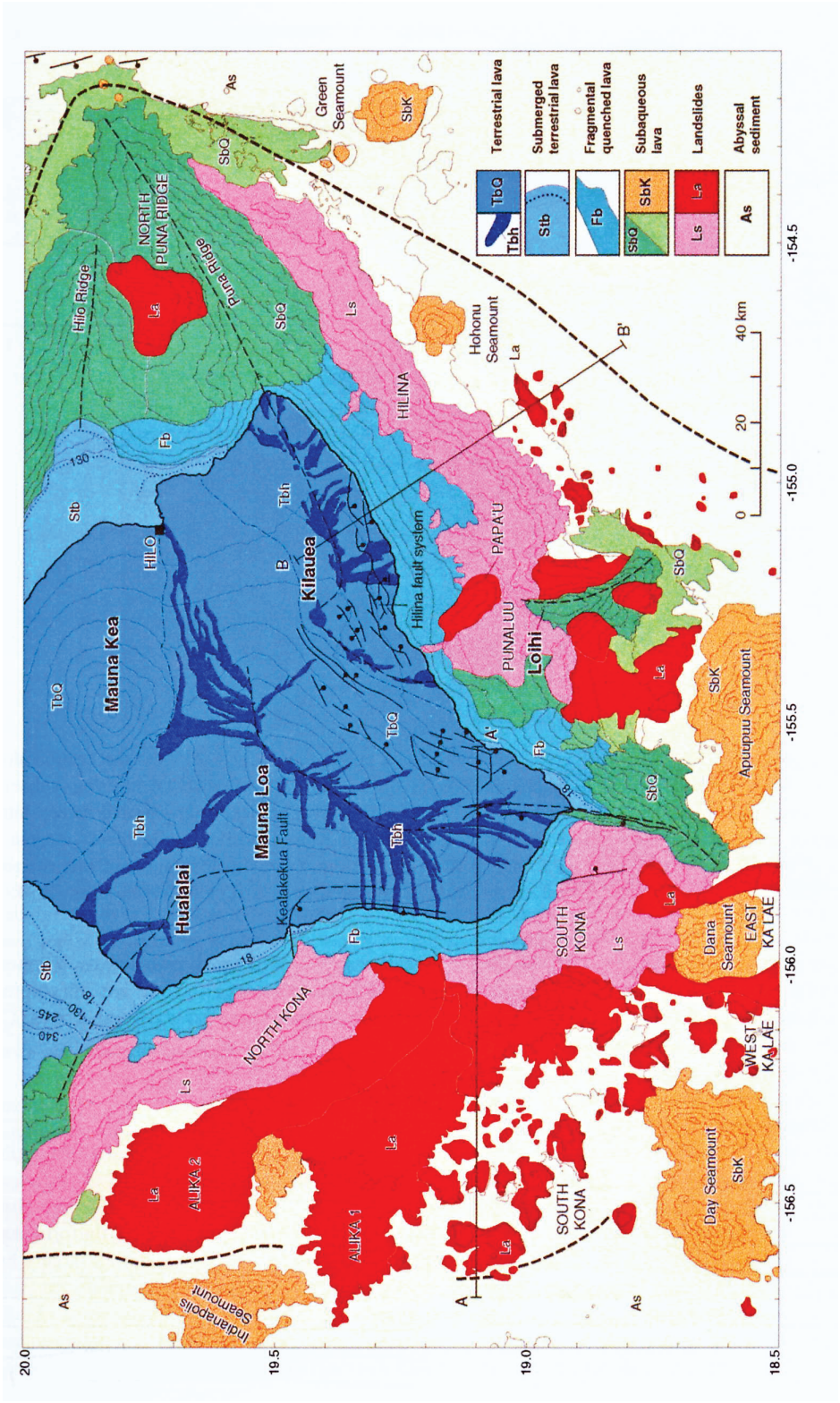
Terrestrial lava
Submerged terrestrial lava
Fragmental quenched lava
Subaqueous lava
Landslides
Abyssal sediment
TbQ
Tbh
Stb
Fb
SbQ
SbK
Ls
La
As
Mauna Kea
Hualalai
Mauna Loa
Kilauea
Loihi
Kealakekua Fault
Hilina fault system
HILINA
PAPA'U
PUNALUU
NORTH PUNA RIDGE
Puna Ridge
Hilo Ridge
Hohonu Seamount
Green Seamount
Apuupuu Seamount
Dana Seamount
Day Seamount
Indianapolis Seamount
NORTH KONA
SOUTH KONA
EAST KA'LAE
WEST KA'LAE
ALIKA 1
ALIKA 2
A
A'
B
B'
0
20
40 km
20.0
19.5
19.0
18.5
-154.5
-155.0
-155.5
-156.0
-156.5

Figure 5.

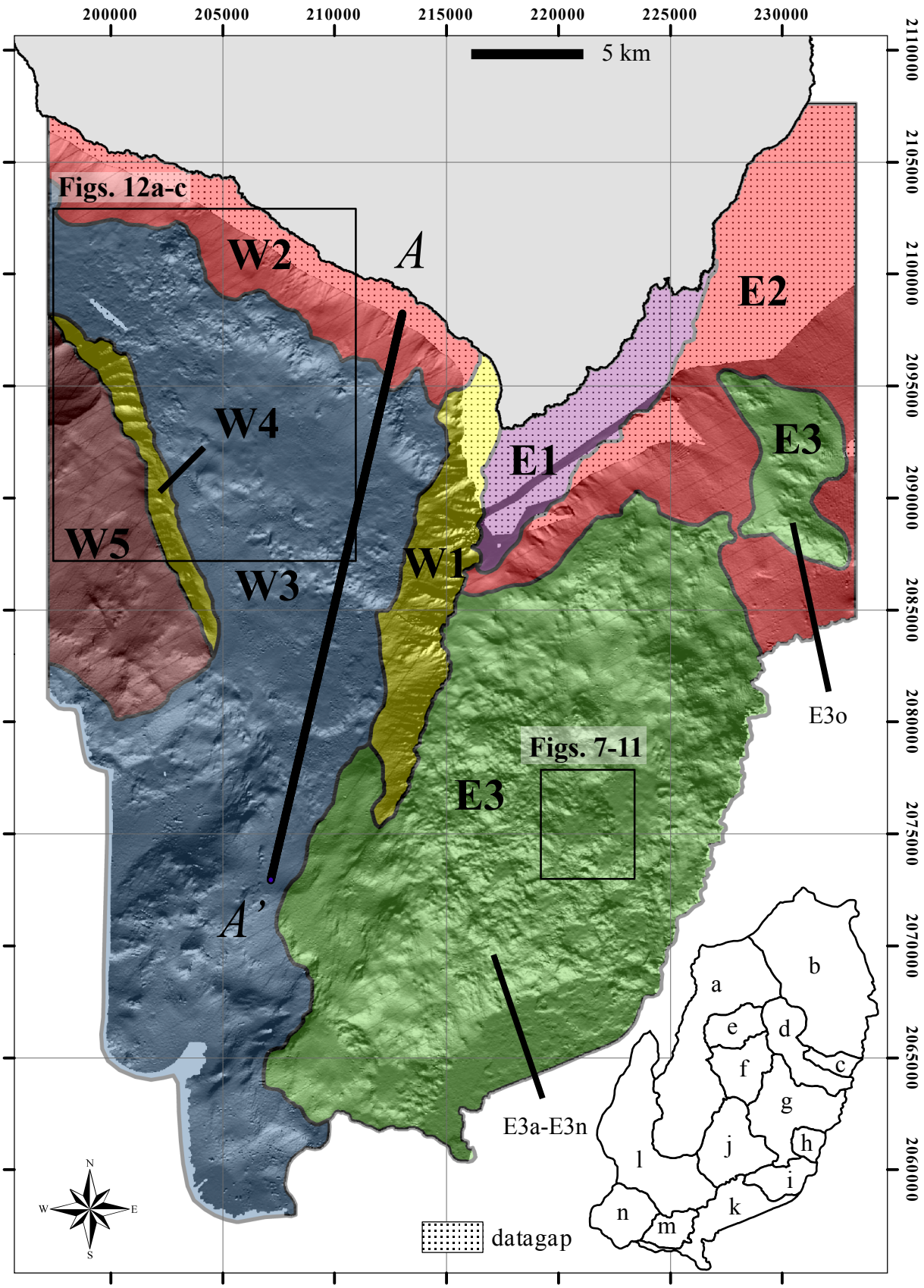
200000
205000
210000
215000
220000
225000
230000
2110000
2105000
2100000
2095000
2090000
2085000
2080000
2075000
2070000
2065000
2060000
5 km
Figs. 12a-c
W2
A
E2
W4
E1
E3
W5
W1
W3
E3o
Figs. 7-11
E3
A'
E3a-E3n
a
b
c
d
e
f
g
h
i
j
k
l
m
n
N
W
E
S
datagap

Figure 6.

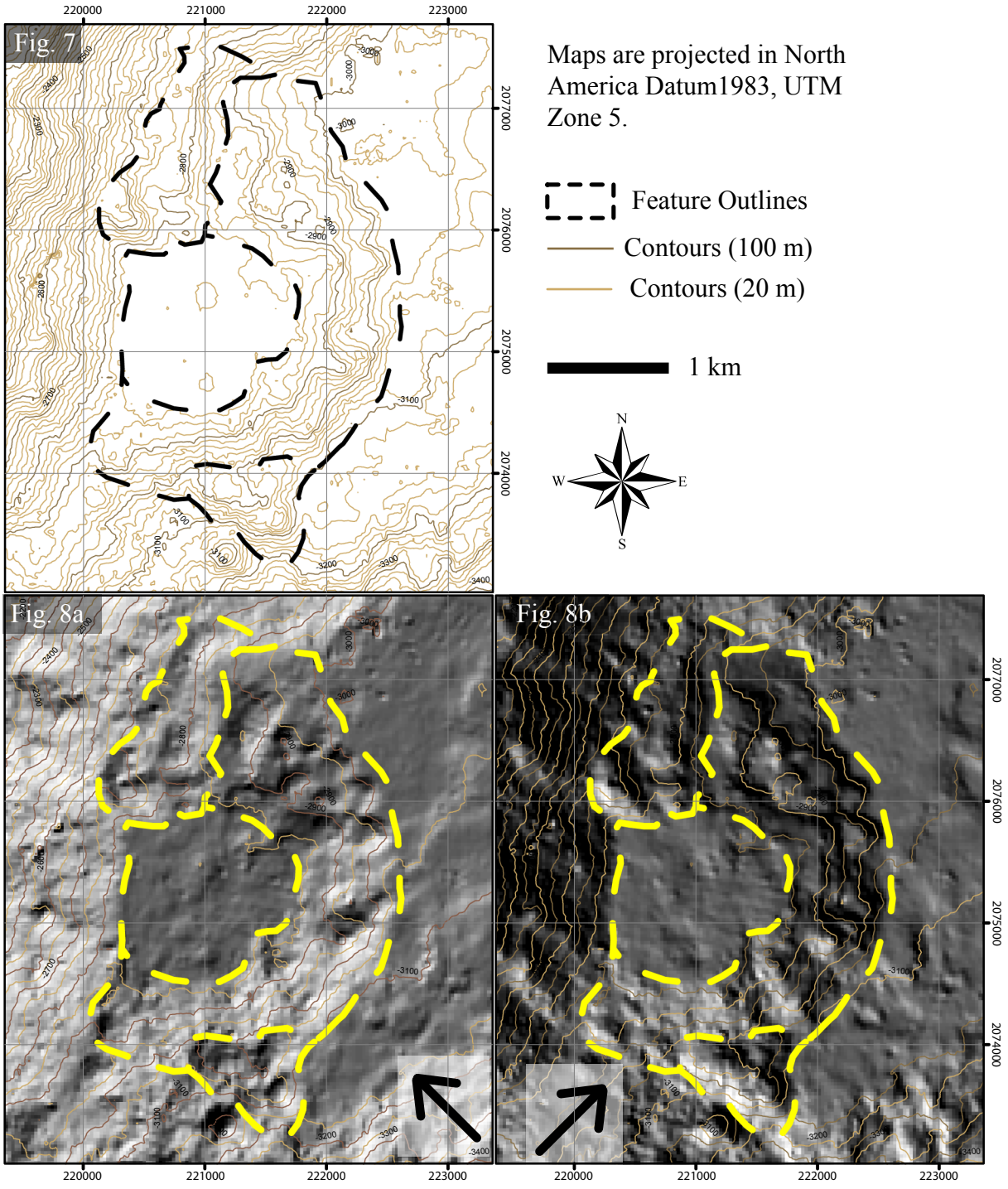
Fig. 7
Fig. 8a
Fig. 8b
Maps are projected in North America Datum1983, UTM Zone 5.
Feature Outlines
Contours (100 m)
Contours (20 m)
1 km
N
W
E
S
220000
221000
222000
223000
2077000
2076000
2075000
2074000
Feature Outlines
Contours (100 m)
Contours (50 m)

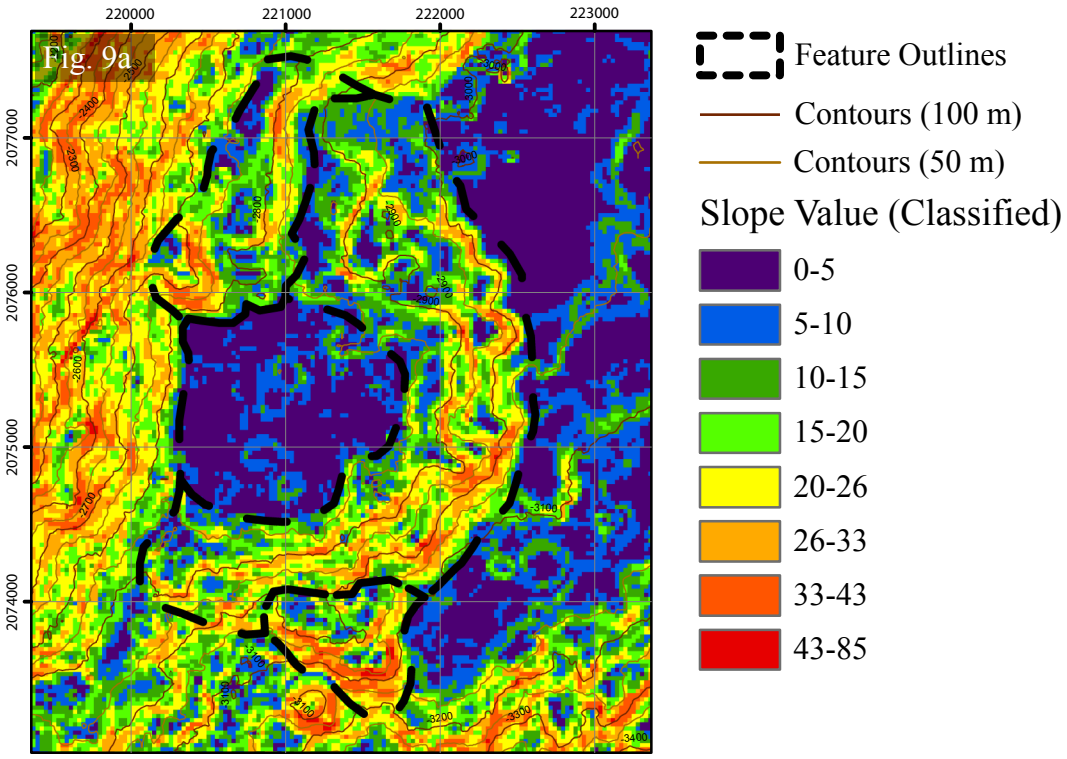
220000
221000
222000
223000
2077000
2076000
2075000
2074000
Fig. 9a
Feature Outlines
Contours (100 m)
Contours (50 m)
Slope Value (Classified)
0-5
5-10
10-15
15-20
20-26
26-33
33-43
43-85

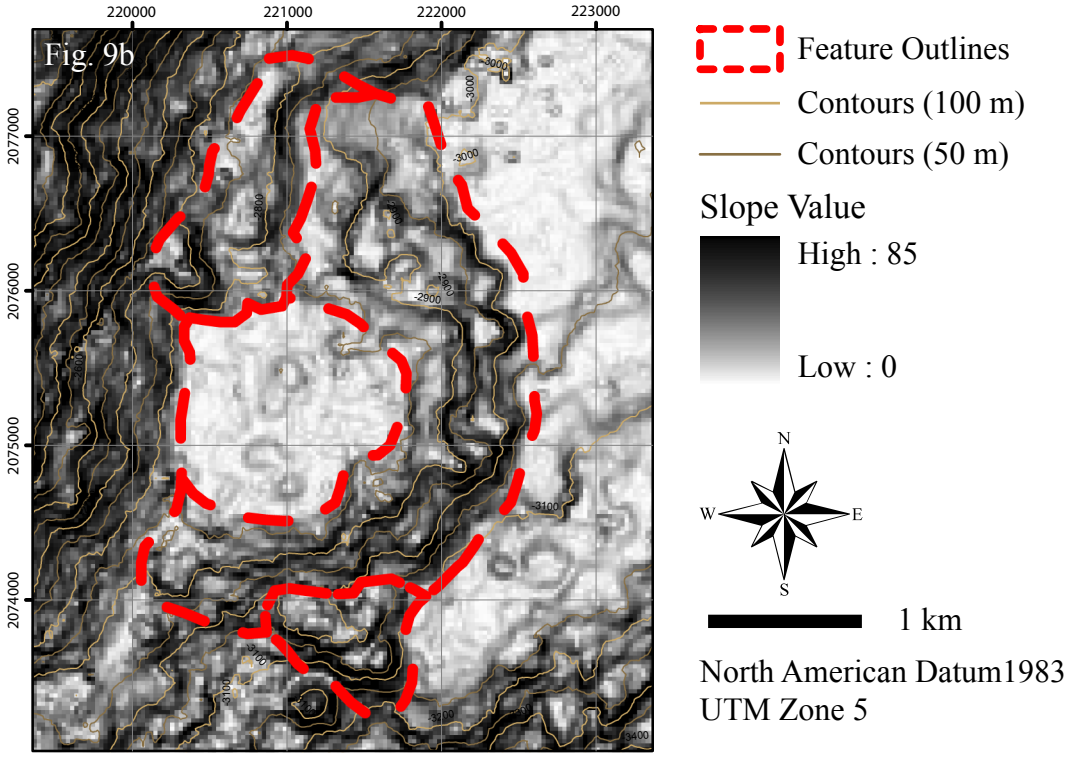
220000
221000
222000
223000
2077000
2076000
2075000
2074000
Fig. 9b
Feature Outlines
Contours (100 m)
Contours (50 m)
Slope Value
High : 85
Low : 0
N
W
E
S
1 km
North American Datum1983
UTM Zone 5

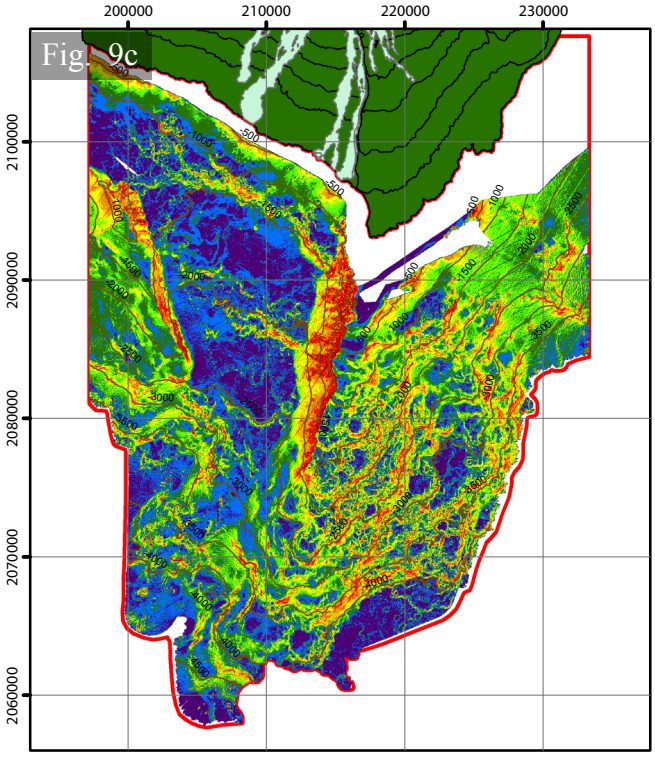

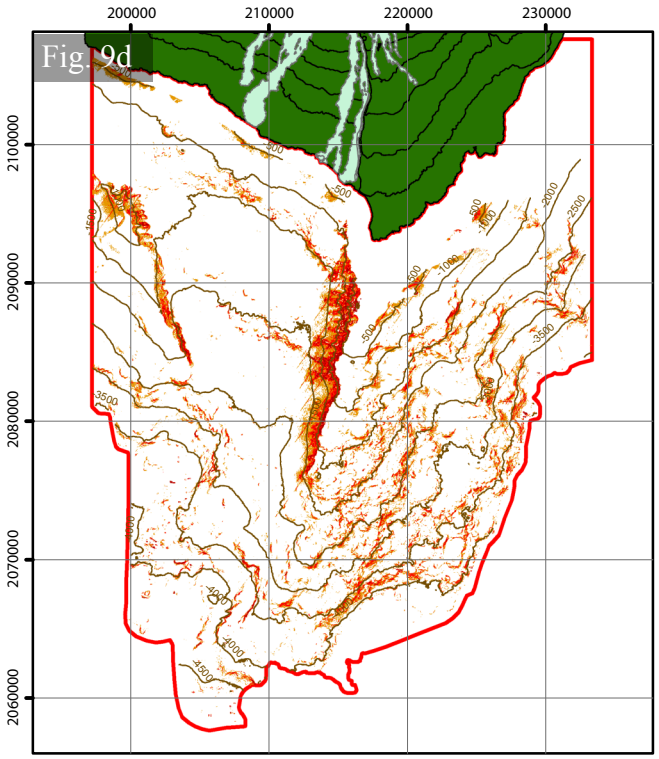

Topographic Contours (100 m)

Bathymetric Contours (500 m)

Study Area

Historical Lava Flows

Subaerial Hawai`i

Slope Value (Classified)

0-5

5-10

10-15

15-20

20-26

26-33

33-43

43-85

N

W E

S

North American Datum1983
UTM Zone 5

10 km

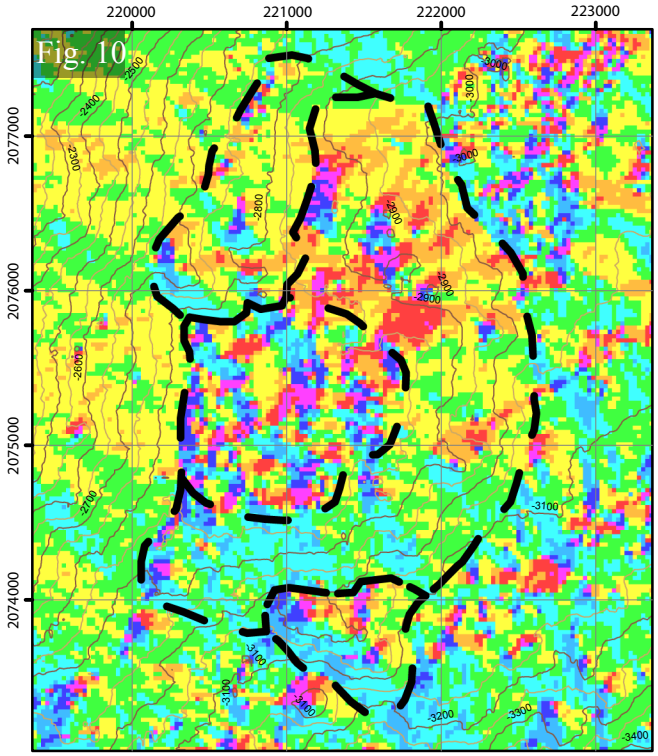

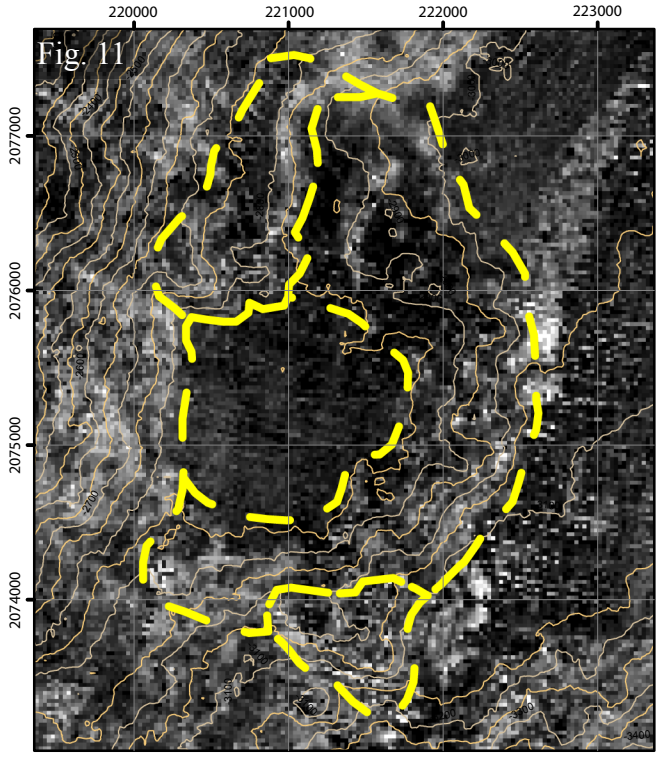

Feature Outlines
Contours (100 m)
Contours (50 m)

Aspect Value

Flat
North (0-22.5)
Northeast (22.5-67.5)
East (67.5-112.5)
Southeast (112.5-157.5)
South (157.5-202.5)
Southwest (202.5-247.5)
West (247.5-292.5)
Northwest (292.5-337.5)
North (337.5-360)

Feature Outlines
Contours (100 m)
Contours (50 m)

Backscatter Value

High : 97

Low : 3.7

N
W
E
S

1 km

North American Datum1983
UTM Zone 5

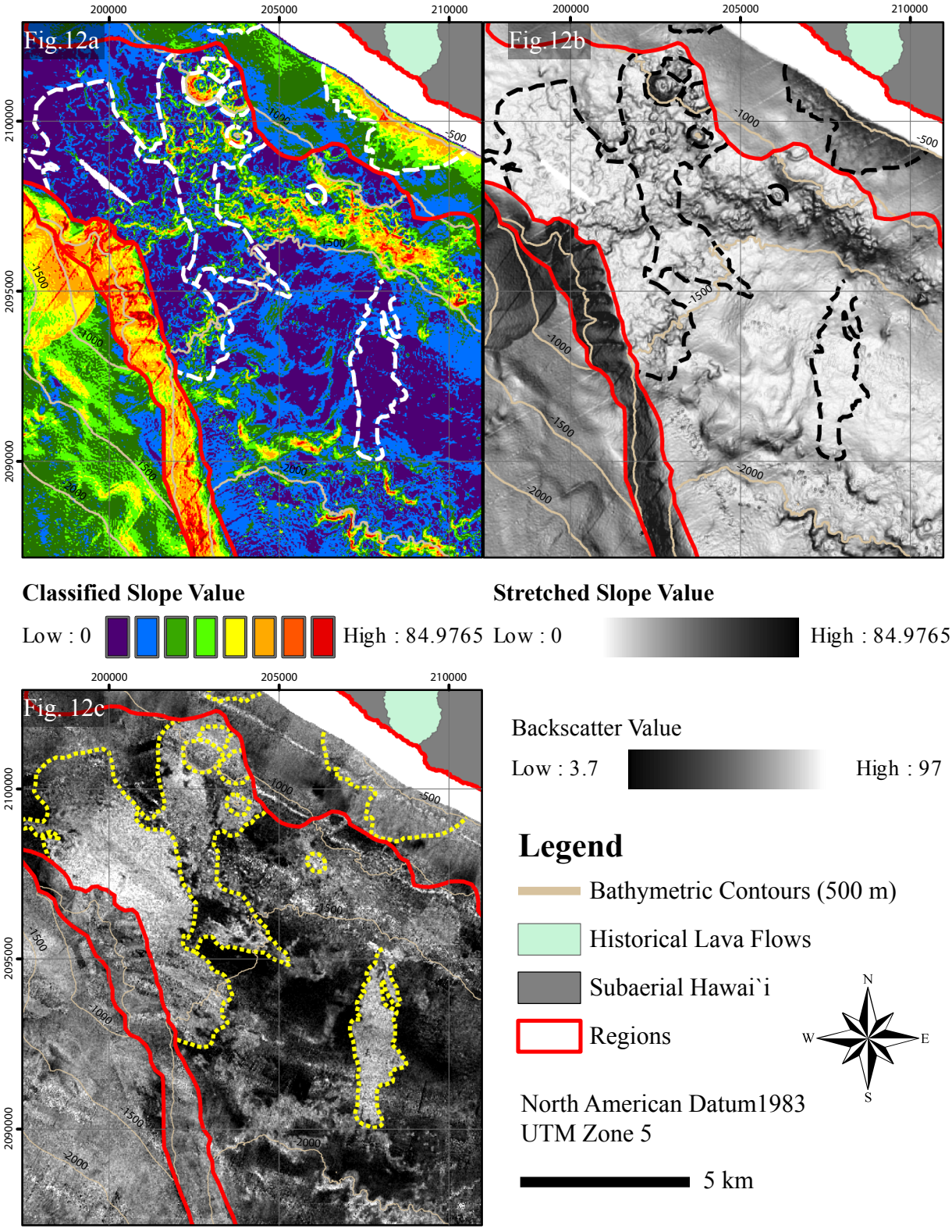
200000
205000
210000
2100000
2095000
2090000
Fig.12a
Fig.12b
-500
-1000
-1500
-2000
Classified Slope Value
Low : 0
High : 84.9765
Stretched Slope Value
Low : 0
High : 84.9765
Fig. 12c
Backscatter Value
Low : 3.7
High : 97
Legend
Bathymetric Contours (500 m)
Historical Lava Flows
Subaerial Hawai`i
Regions
N
W
E
S
North American Datum1983
UTM Zone 5
5 km

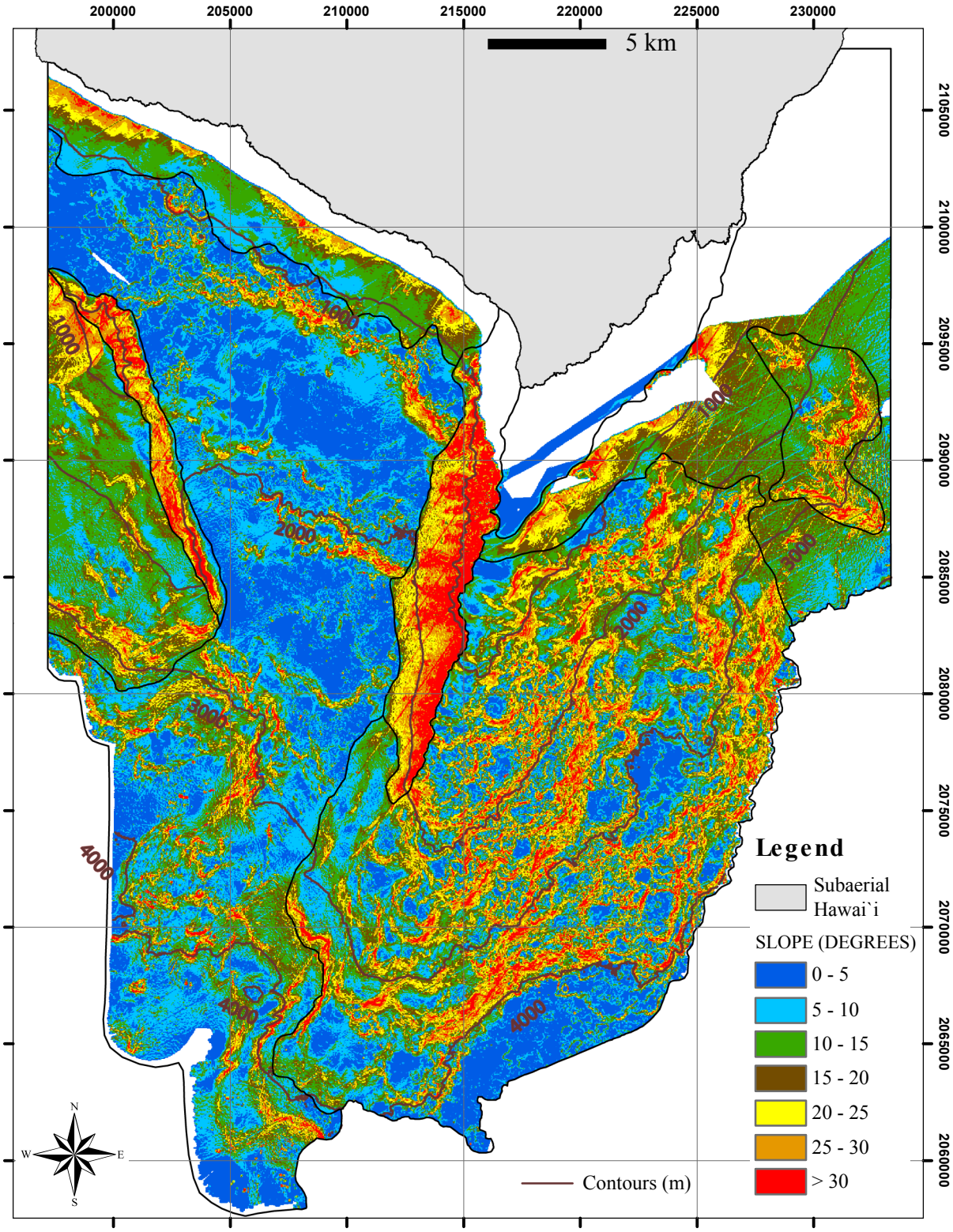
200000
205000
210000
215000
220000
225000
230000
5 km
2105000
2100000
2095000
2090000
2085000
2080000
2075000
2070000
2065000
2060000
1000
2000
3000
4000
Legend
Subaerial Hawai`i
SLOPE (DEGREES)
0 - 5
5 - 10
10 - 15
15 - 20
20 - 25
25 - 30
> 30
Contours (m)
N
W
E
S

Figure 13a.

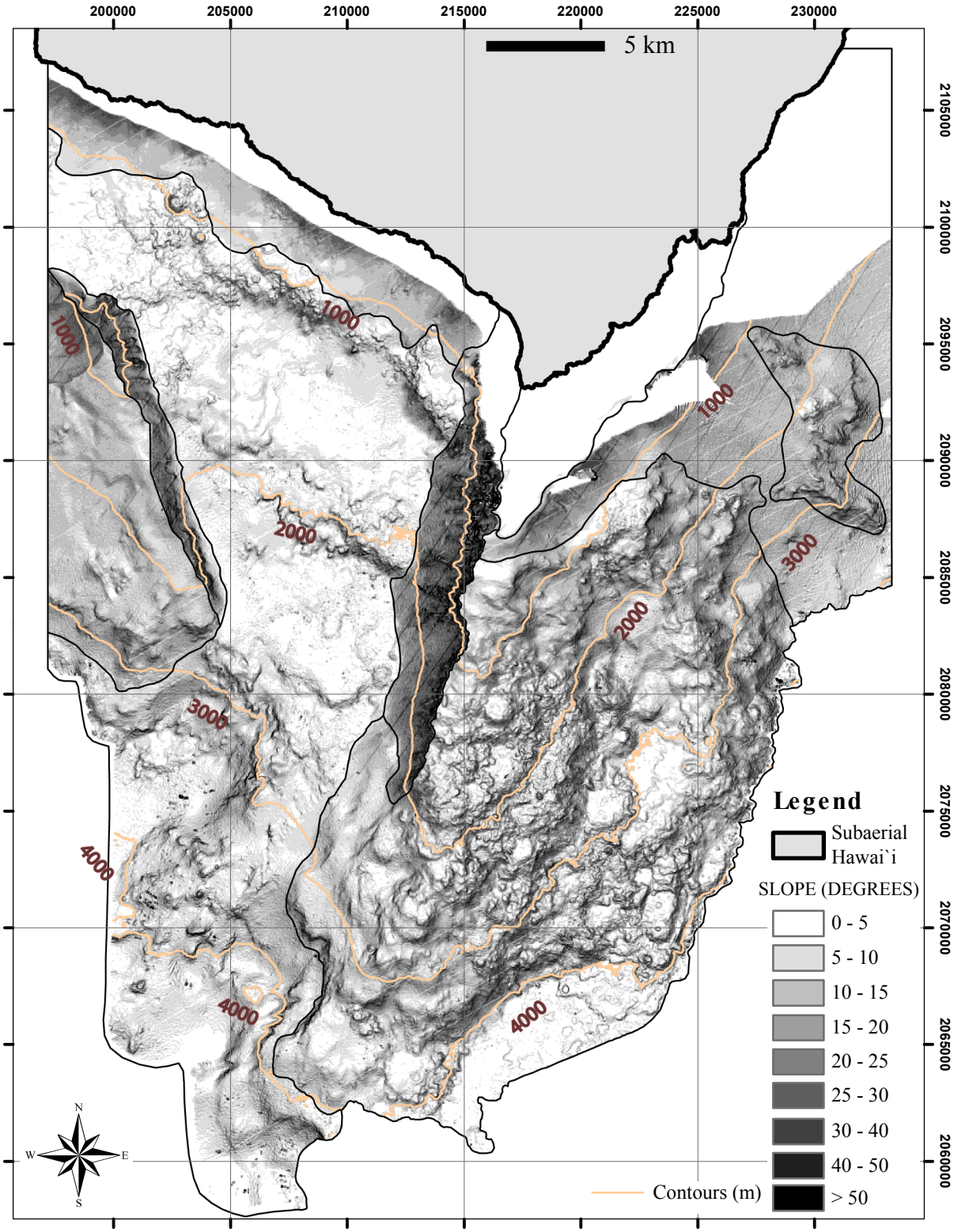
200000
205000
210000
215000
220000
225000
230000
2105000
2100000
2095000
2090000
2085000
2080000
2075000
2070000
2065000
2060000
5 km
1000
2000
3000
4000
N
W
E
S
Legend
Subaerial Hawai`i
SLOPE (DEGREES)
0 - 5
5 - 10
10 - 15
15 - 20
20 - 25
25 - 30
30 - 40
40 - 50
> 50
Contours (m)

Figure 13b.

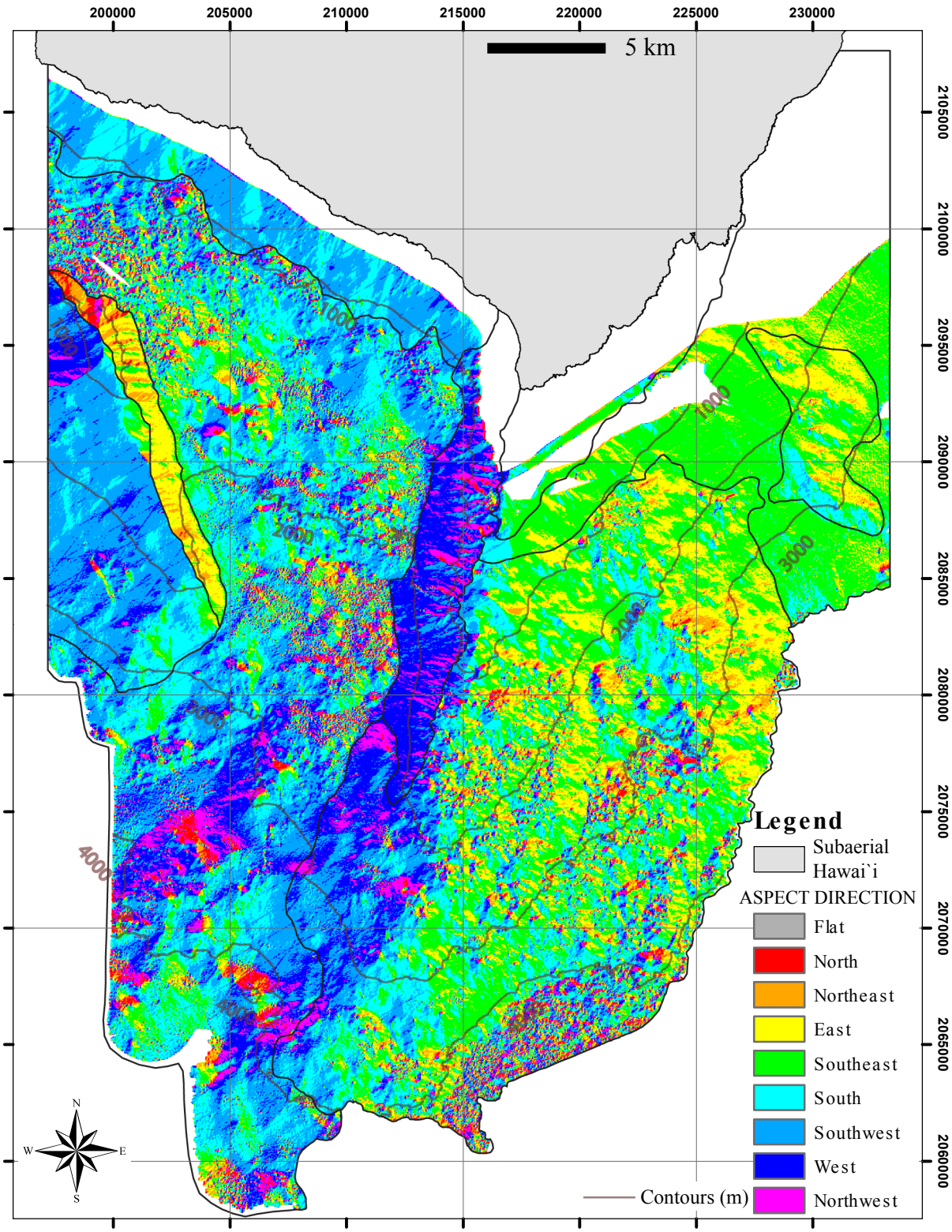
200000
205000
210000
215000
220000
225000
230000
5 km
2105000
2100000
2095000
2090000
2085000
2080000
2075000
2070000
2065000
2060000
1000
2000
3000
4000
Legend
Subaerial
Hawai`i
ASPECT DIRECTION
Flat
North
Northeast
East
Southeast
South
Southwest
West
Northwest
Contours (m)
N
W
E
S

Figure 14.

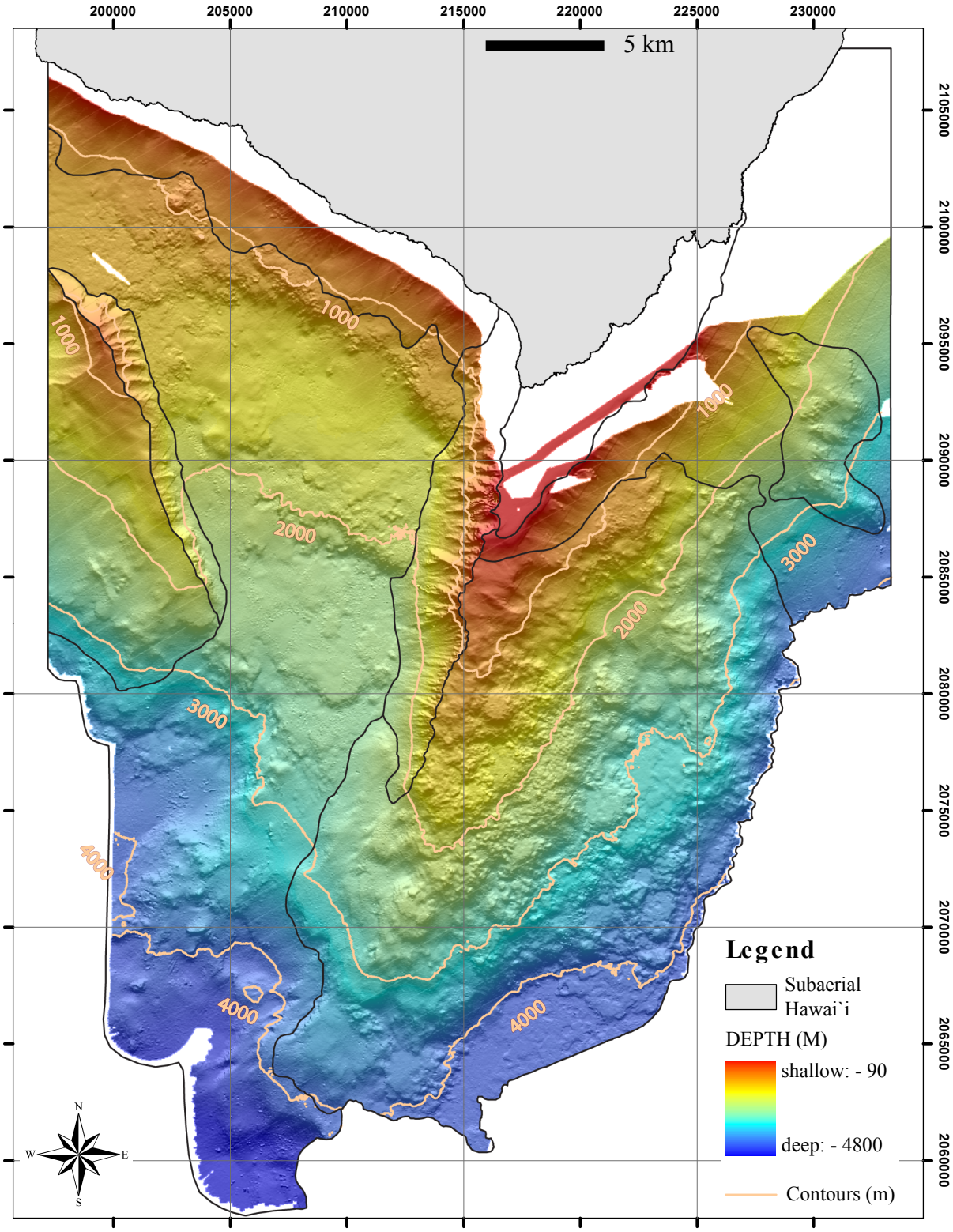
200000
205000
210000
215000
220000
225000
230000
2105000
2100000
2095000
2090000
2085000
2080000
2075000
2070000
2065000
2060000
5 km
1000
2000
3000
4000
N
W
E
S
Legend
Subaerial Hawai`i
DEPTH (M)
shallow: - 90
deep: - 4800
Contours (m)

Figure 15.

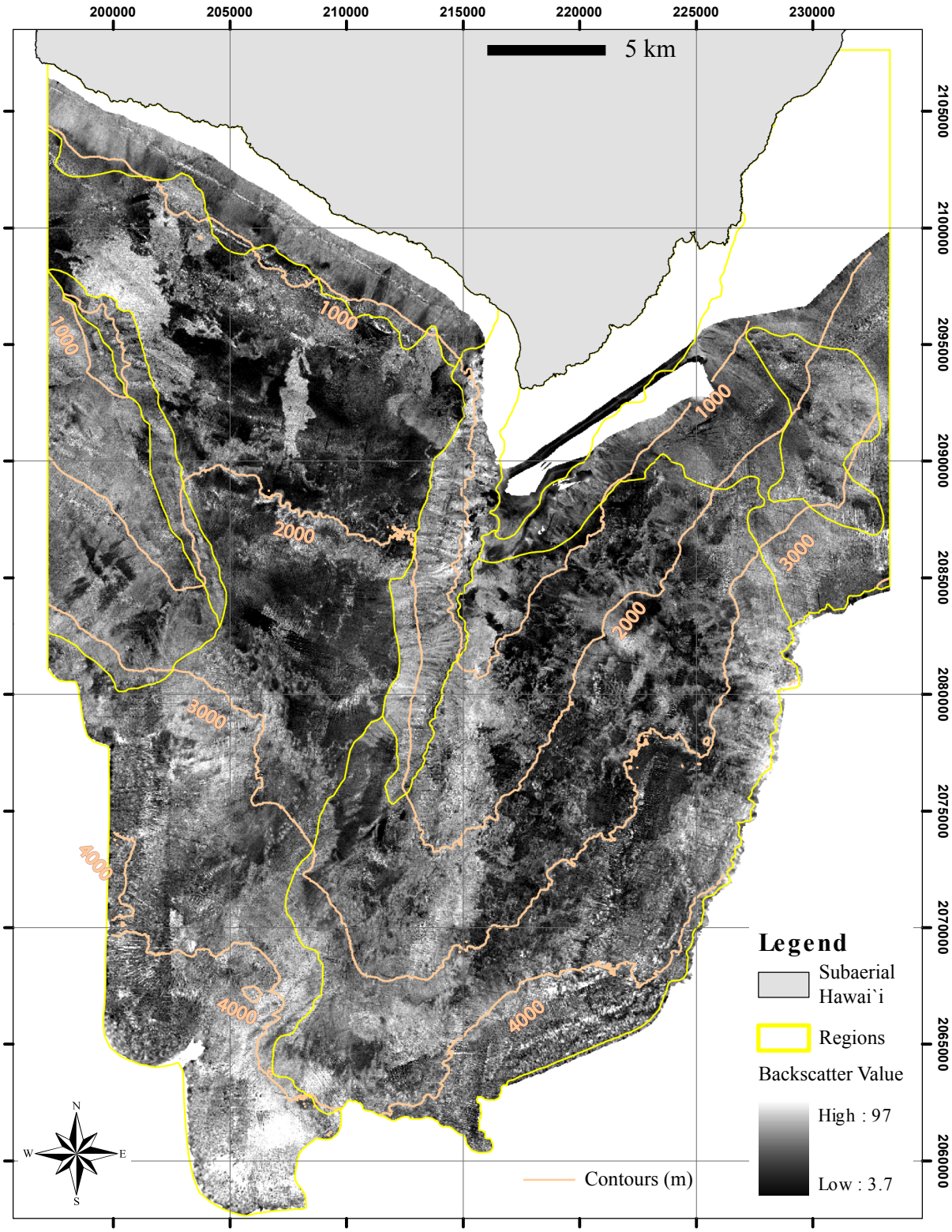
200000
205000
210000
215000
220000
225000
230000
5 km
2105000
2100000
2095000
2090000
2085000
2080000
2075000
2070000
2065000
2060000
1000
2000
3000
4000
N
W
E
S
Legend
Subaerial Hawai`i
Regions
Backscatter Value
High : 97
Low : 3.7
Contours (m)

Figure 16.

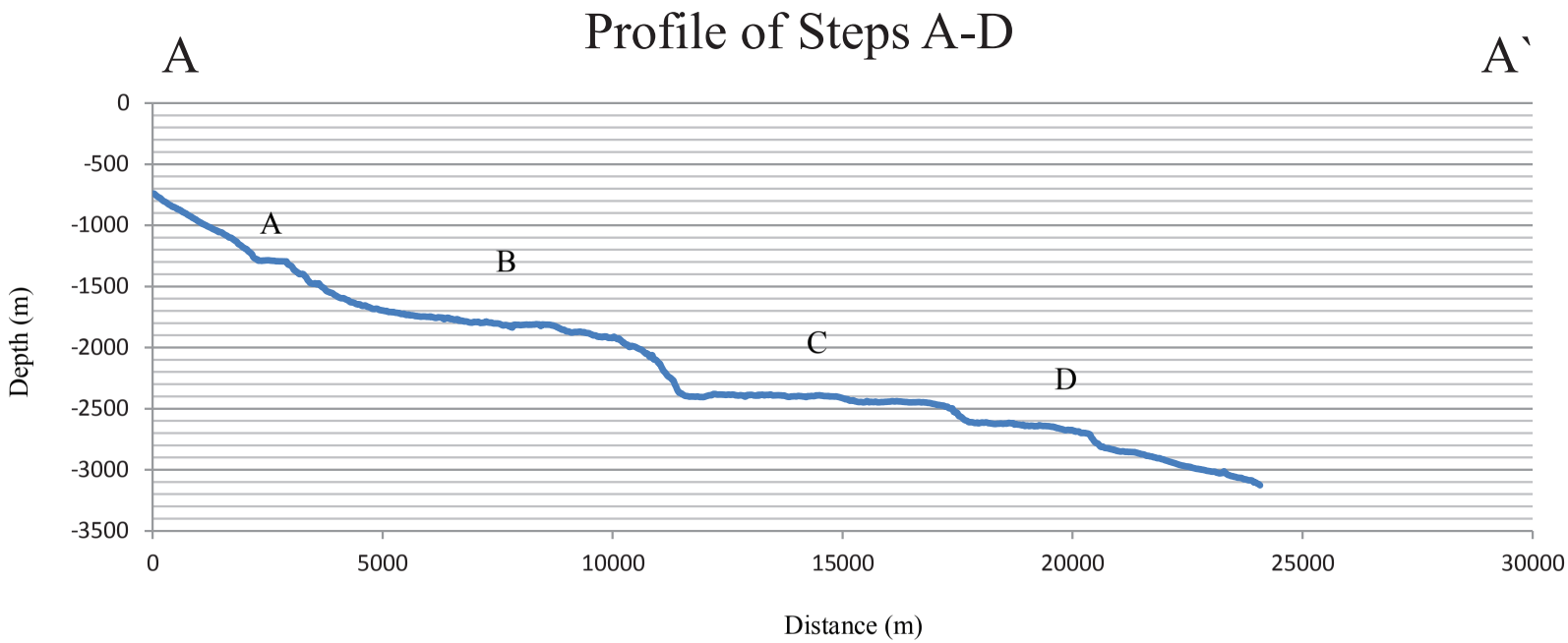
Profile of Steps A-D
A
A`
0
-500
-1000
-1500
-2000
-2500
-3000
-3500
Depth (m)
A
B
C
D
0
5000
10000
15000
20000
25000
30000
Distance (m)

Figure 17.

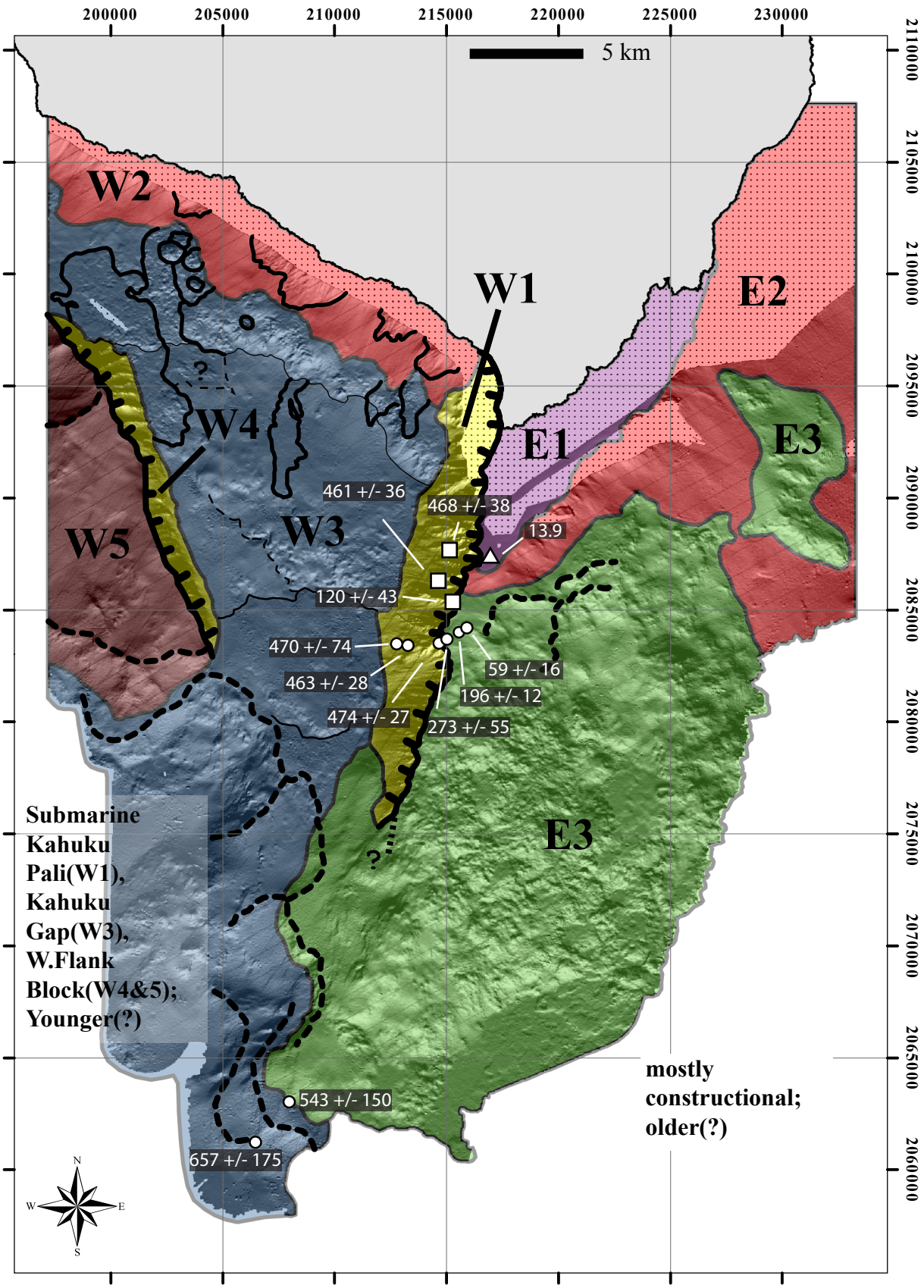
200000
205000
210000
215000
220000
225000
230000
2110000
2105000
2100000
2095000
2090000
2085000
2080000
2075000
2070000
2065000
2060000
5 km
W1
W2
W3
W4
W5
E1
E2
E3
461 +/- 36
468 +/- 38
13.9
120 +/- 43
470 +/- 74
463 +/- 28
474 +/- 27
59 +/- 16
196 +/- 12
273 +/- 55
543 +/- 150
657 +/- 175
Submarine Kahuku Pali(W1), Kahuku Gap(W3), W.Flank Block(W4&5); Younger(?)
mostly constructional; older(?)
N
W
E
S

Figure 18a.

The submarine Kahuku Pali (west-facing scarp).

Nearshore region that's mantled by volcaniclastic. Region includes shoreline -crossing lava flows (as young as the 1868 & 1887?).

The Kahuku Gap. It's northern shallower half includes broad steps A, B, C, and D. It's southern deeper half is marked by concave-seaward scarps.

The east-facing scarp of the West-flank block.

The west-facing slopes of the West-flank block.

The submerged portion of Mauna Loa's subaerial flank.

Nearshore region that appears to be mantled by volcaniclastics like region W2.

Region that is primarily constructional. E3 exhibits the classic rugged morphology of Hawaiian submarine rift zones (e.g., areas with abundant volcanic cones and pillow mounds).

datagap

Steps A-D; seaward margin

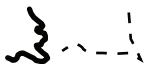

Lava flows/Cones

Less well-defined scarps

Well-defined scarps

Age (ka)

△ Moore et al. (1990)

□ Garcia et al. (1995) PV dives; age data from Jicha et al. (2012)

○ Jason dives; age from Jicha et al. (2012)

Figure 18b. Expanded explanation of the geologic map.

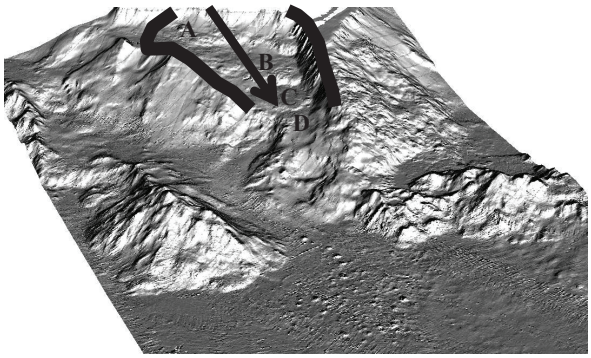

Stage 1a:
-removed most of the material
-likely catastrophic
Stage 1b:
-subsequent volcanic activity and depositional processes partially resurfaced the gap's floor and appears to be ongoing

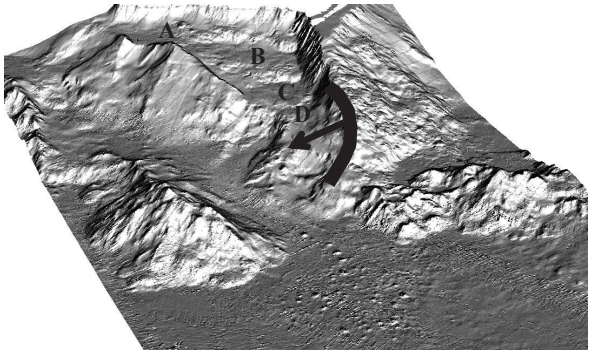

Stage 2:
-part of the Eastern flank slumped on top of the Kahuku Gap's step D
-slumping episode appears to bury the southern end of the submarine Kahuku Pali

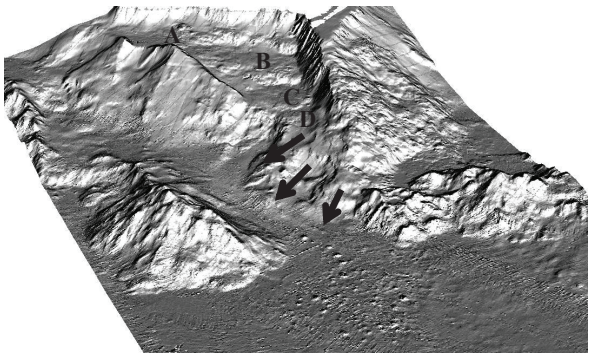

Stage 3:
-failure(s) generated concave-seaward scarps that cut into step D and the south-southwest tip of the Eastern flank.

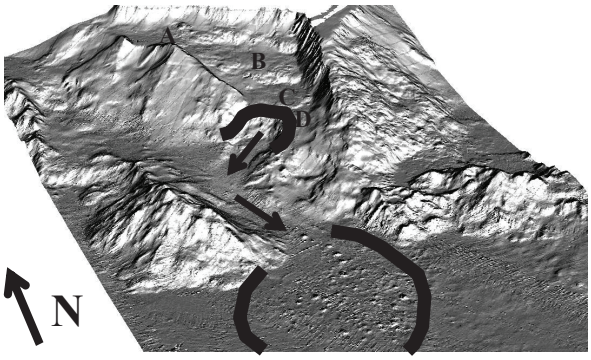

Stage 4:
-debris avalanche generated a ~700 m-deep amphitheater, a debris chute, and a broad field of hummocks (blocks ~1 km and less across)

Figure 19.

APPENDIX A

The general descriptions of E3's sub-regions (E3a-E3o).

Sub-region	Depth (m)	Area (km)	Well-defined features?
E3a	~420 to ~3,000	~73	n/a
E3b	~900 to ~4,000	~80	n/a
E3c	~3,000 to ~4,000	~5	cone 1
E3d	~2,180 to ~4,000	~21	cones 2 and 3
E3e	~1,210 to ~2,550	~12	cone 4
E3f	~1,680 to ~3,000	~18	n/a
E3g	~2,815 to ~4,150	~33	cone 5
E3h	~3,700 to ~4,100	~5	cones 6 and 7
E3i	~3,800 to ~4,100	~11	cone 8
E3j	~2,425 to ~4,100	~26	cone 9
E3k	~3,900 to ~4,100	~22	n/a
E3l	~2,200 to ~4,100	~56	n/a
E3m	~3,800 to ~4,100	~9	cone 10
E3n	~3,300 to ~4,025	~17	cone 11
E3o	~1,050 to ~3,850	~30	n/a

The sizes of selected well-defined cones in E3's sub-regions.

Sub-region, Feature	Height (H), m	Basal Diameter (D), m	Top Diameter (d), m	Flatness (d/D), m	Height-to-diameter ratio (H/D), m
E3c, cone 1	120	1,200	850	0.71	0.10
E3d, cone 2	700	3,000	810	0.27	0.23
E3d, cone 3	315	1,810	540	0.30	0.17
E3e, cone 4	340	2,220	1,090	0.49	0.15
E3g, cone 5	290	3,730	2,060	0.55	0.08
E3h, cone 6	210	2,045	1,410	0.69	0.10
E3h, cone 7	200	1,630	870	0.53	0.12
E3i, cone 8	335	1,820	1,215	0.67	0.18
E3j, cone 9	120	1,520	1,040	0.68	0.08
E3m, cone 10	360	5,120	2,090	0.41	0.07
E3n, cone 11	600	6,765	3300	0.49	0.09

The following page is the location map of the sub-regions' selected cones. Sub-regions are also shown in Figure 6.

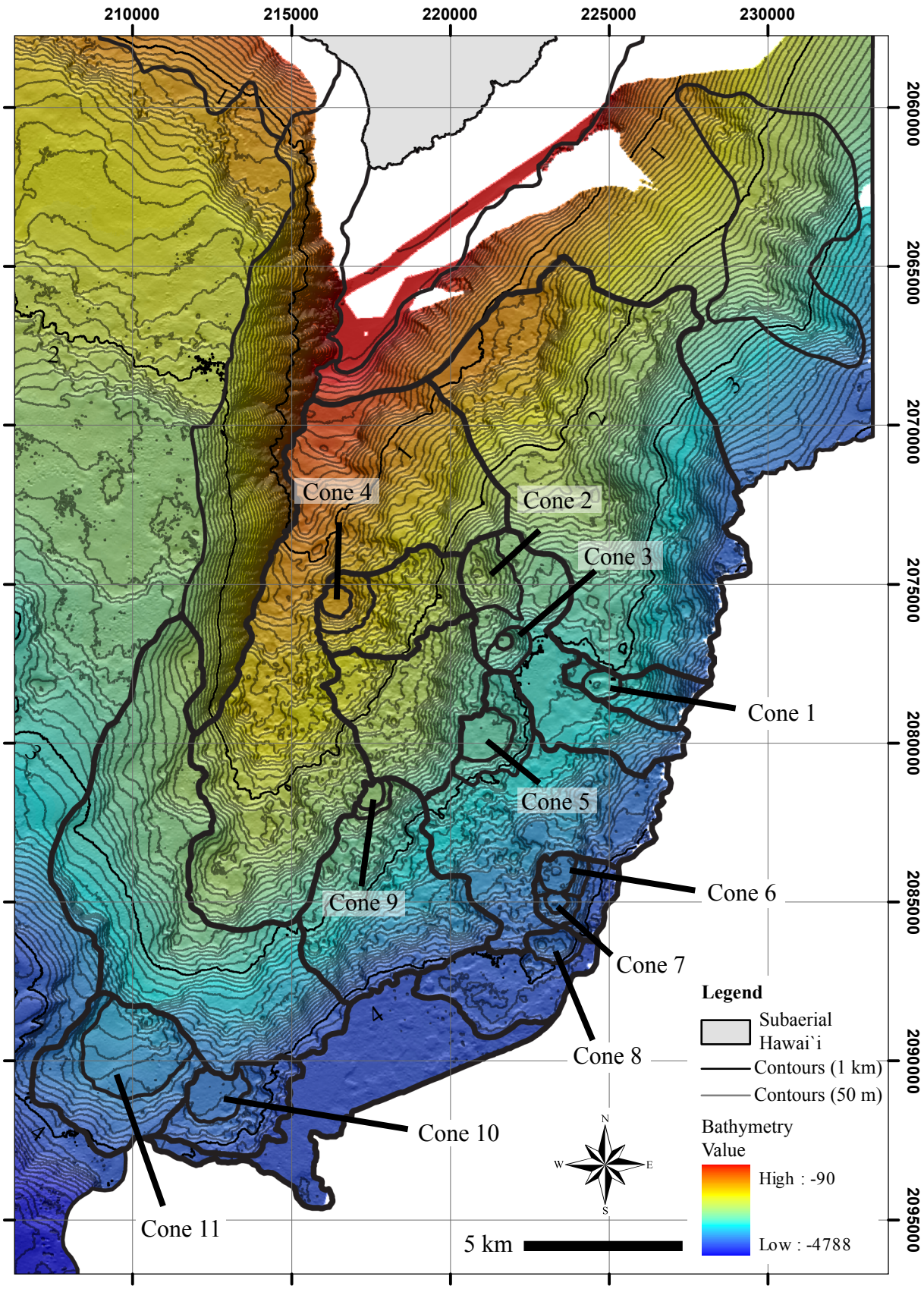

Appendix A (continued)

APPENDIX B

Volume calculations for the Kahuku Gap's Stage 1a:

ArcGIS's Cut/Fill and Surface Volume tools were used to calculate the volume of material assumed to have been removed during Stage 1a. It is important to note that we only attempted to obtain a rough estimate. Bathymetric data that were used can be downloaded from the University of Hawai'i's School of Ocean Earth Science and Technology/Hawaii Mapping Research Group website http://www.soest.hawaii.edu/HMRG/Multibeam/grids.php#50mBathy.

Steps (generalized) used to calculate volumes are as follows:

1) Created a shapefile (area outlined below in thick black line; left image) and edited its attribute table (gave two depth values; 0 and -2,660 m). Depth values based on the 50 m DEM (right image).

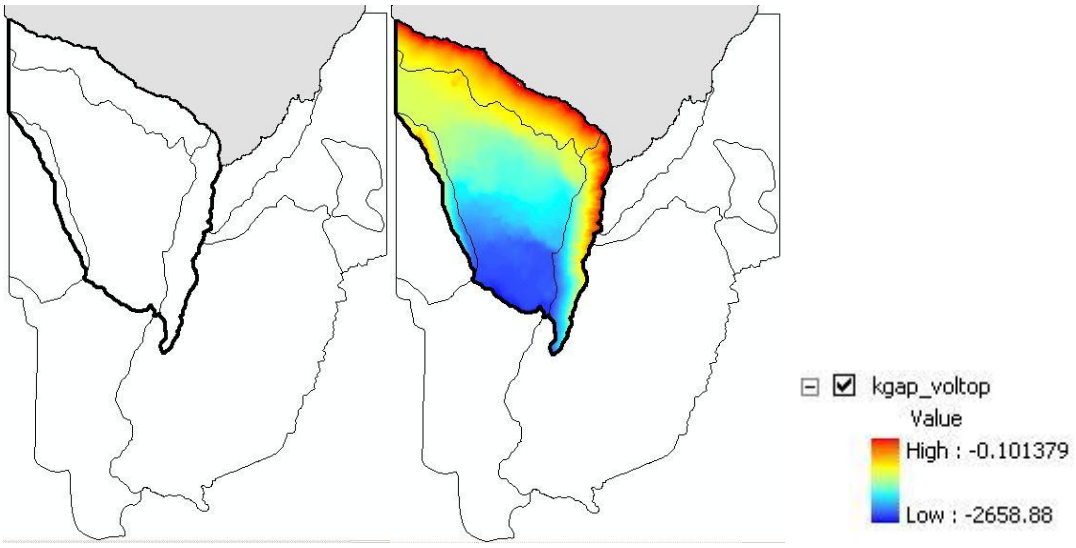

2) Created two rasters from the shapefile using 0 and -2,660 m depth values.

3) Used Cut/Fill to calculate the volume of the area between 0 and -2,660 m.

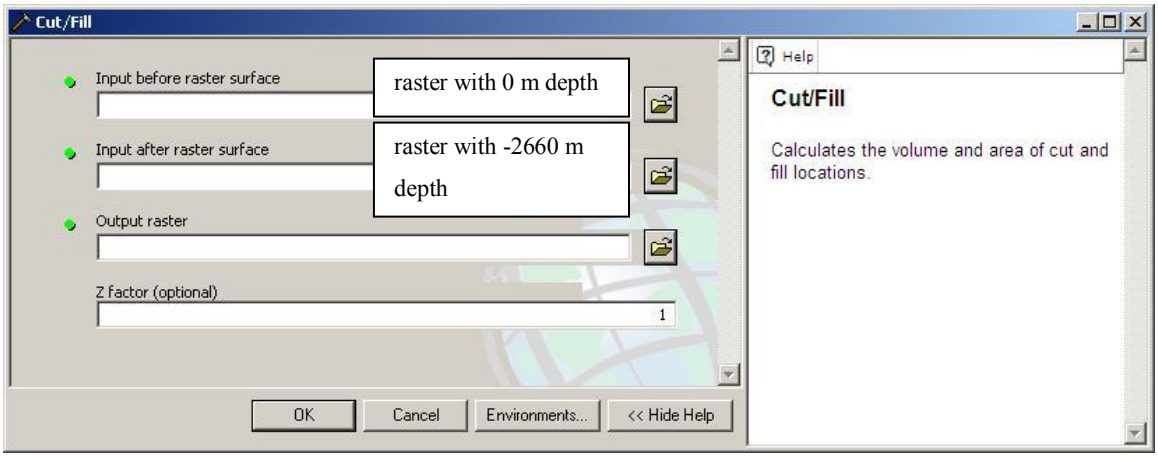

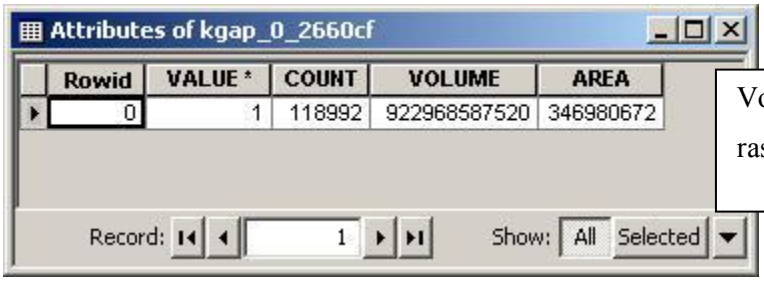

Volume of the output raster: ~923 km^3

4) Used Surface Volume (from 3D Analyst -> Functional Surface) to calculate the volume of material above -2,660 m. For a detailed explanation of the Surface Volume tool, refer to the following URL: http://resources.esri.com/help/9.3/arcgisdesktop/com/gp_toolref/3d_analyst_tools/how_surface_volume_3d_analyst_works.htm.

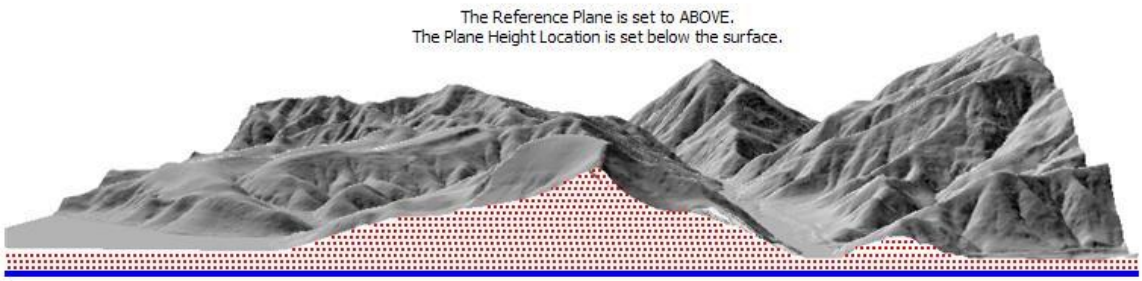

(image is from ESRI website above)

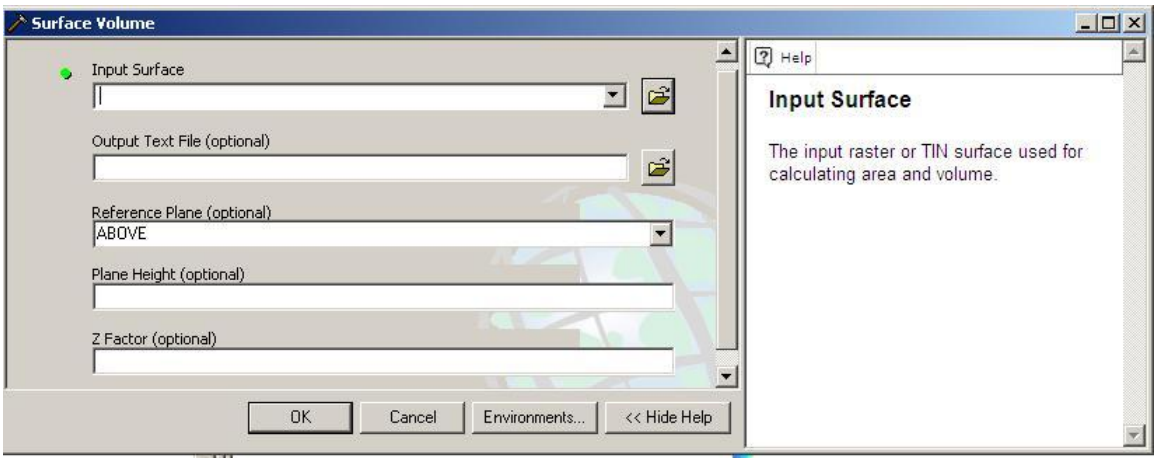

Below is the output text file

```
1  Dataset, Plane_Height, Reference, Z_Factor, Area_2D, Area_3D, Volume
2  ..thymetry_Version19\kgap_voltop, -2660.00, ABOVE, 1.000000,
   343174860.0154, 363967850.73538, 414562879094.45
3
```

Volume: ~415 km^3

5) Steps 1-4 summarized

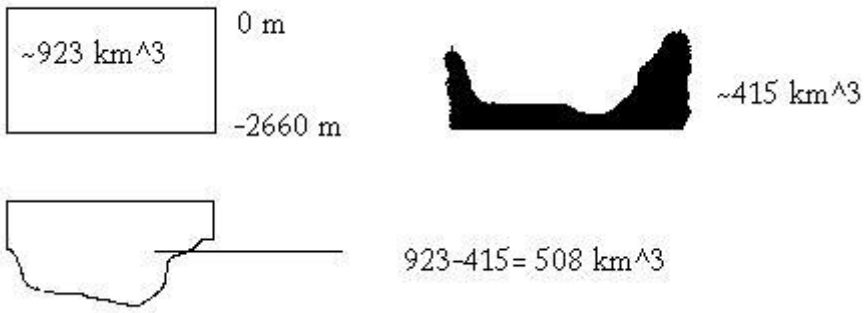

6) Modified steps 1-4 to calculate for a lower estimate. Created a TIN (right image) and a raster from the TIN (left image).

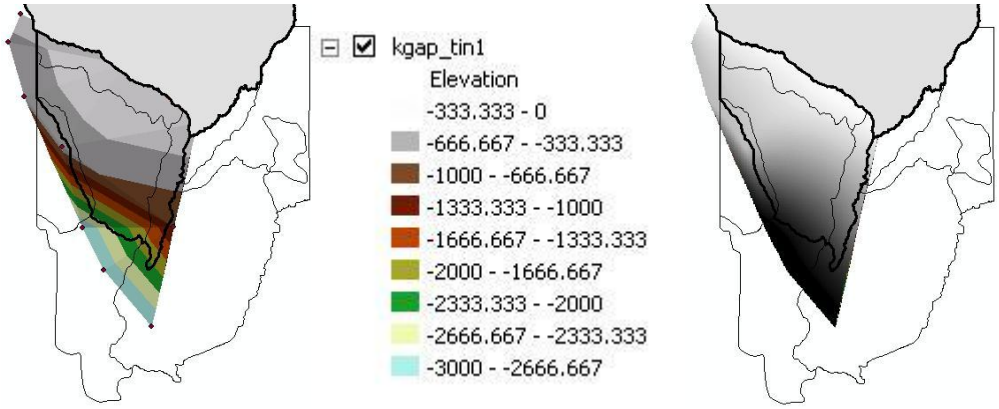

Extracted the new bathymetry created from theTIN.

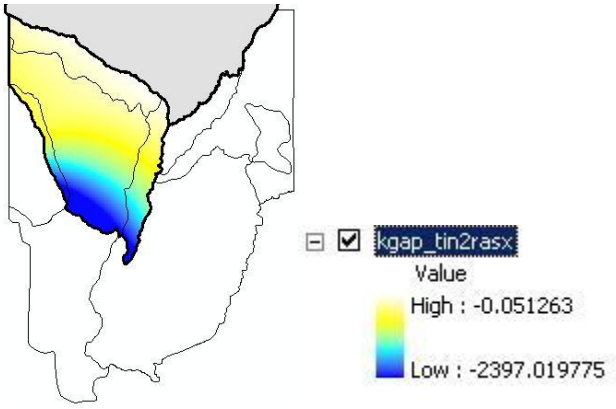

Used Cut/Fill

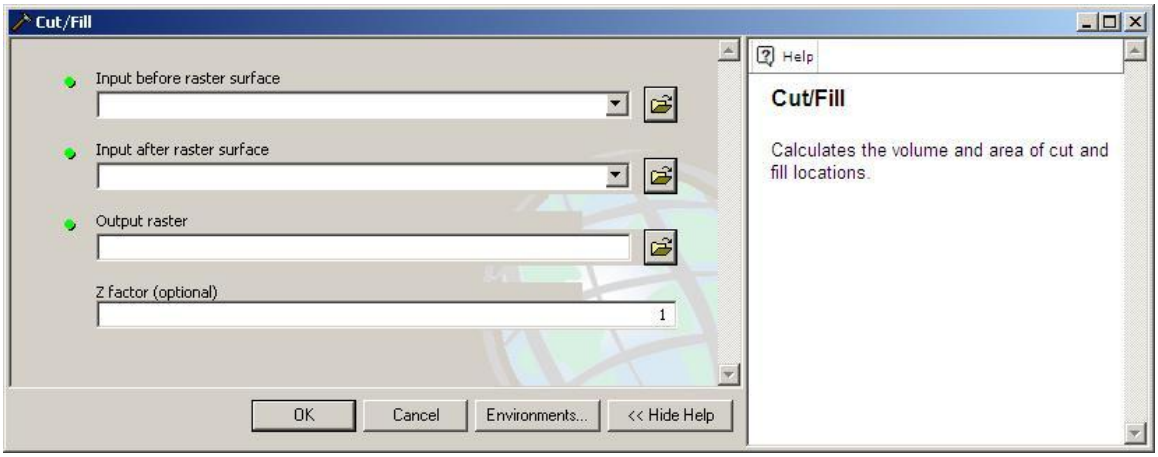

Output Volume from Cut/Fill

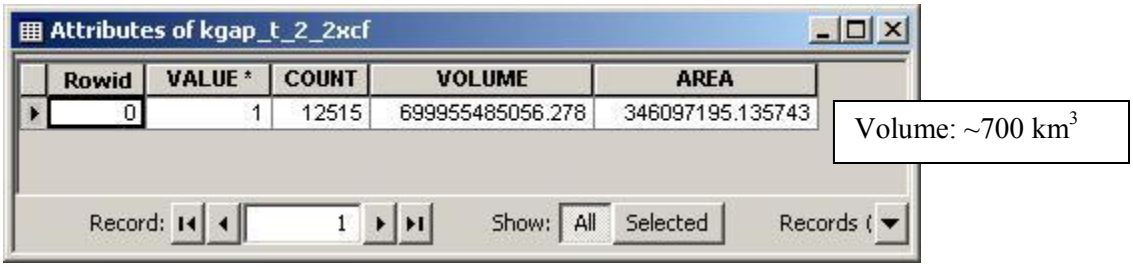

7) Lower volume calculation summarized.

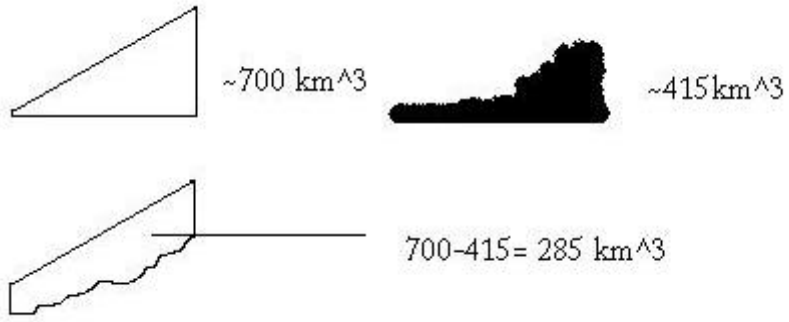

8) Rounded volume estimates to ~300-500 km^3.

REFERENCES CITED

Barnard, W. M., 1995, Mauna Loa volcano; Historical eruptions, exploration, and observations (1779-1910), *in* Rhodes, J. M., and Lockwood, J. P., eds., Mauna Loa Revealed: Structure, Composition, History, and Hazards: American Geophysical Union Geophysical Monograph 92, 1-19.

Chadwick, W. W., Jr., Embley, R. W., Johnson, P. D., Merle, S. G., and Ristau, S., 2005, The submarine flanks of Anatahan Volcano, Commonwealth of the Northern Mariana Islands: Journal of Volcanology and Geothermal Research, v. 146 (1-3), 8-25, doi:10.1016/j.jvolgeores.2004.11.032.

Chadwick, W. W., Jr., Moore, J. G., Garcia, M. O., and Fox, C. G., 1993, Bathymetry of southern Mauna Loa volcano, Hawaii: U.S. Geological Survey Miscellaneous Field Studies Map MF-2233, scale 1:150,000, 1 sheet.

Clague, D. A., and Dalrymple, G. B., 1987, The Hawaiian-Emperor volcanic chain; Part I; Geologic evolution: U.S. Geological Survey Professional Paper 1350, v. 1, 5-54.

Clague, D. A., and Dalrymple, G. B., 1989, Tectonics, geochronology, and origin of the Hawaiian-Emperor volcanic chain, *in* Winterer, E. L., Hussong, D. M., and Decker, R. W., eds., The Geology of North America: The eastern Pacific Ocean and Hawaii: Geological Society of America, v. N, 188-217.

Clague, D. A., Moore, J. G., and Reynolds, J. R., 2000, Formation of submarine flat-topped volcanic cones in Hawai‘i: Bulletin of Volcanology, v. 62 (3), 214-233, doi:10.1007/s004450000088.

Eakins, B. W., and Robinson, J. E., 2006, Submarine geology of Hana Ridge and Haleakala volcano northeast flank, Maui: Journal of Volcanology and Geothermal Research, v. 151 (1-3), 229-250, doi:10.1016/j.jvolgeores.2005.07.034.

Eakins, B. W., Robinson, J. E., Kanamatsu, T., Naka, J., Smith, J. R., Takahashi, E., and Clague, D. A., 2003, Hawaii's volcanoes revealed: U.S. Geological Survey Geologic Investigations Series I-2809, 1 sheet, URL:http://geopubs.wr.usgs.gov/i-map/i2809/ (accessed June 2007).

Flinders, A. F., Ito, G., and Garcia, M. O., 2010, Gravity anomalies of the northern Hawaiian Islands; Implications on the shield evolutions of Kauai and Niihau: Journal of Geophysical Research, v. 115 (B8), B08412, doi:10.1029/2009JB006877.

Fornari, D. J., and Campbell, J. F., 1987, Submarine topography around the Hawaiian Islands, *in* Decker, R. W., Wright, T. L., and Stauffer, P. H., eds., U.S. Geological Survey Professional Paper 1350, v. 1, 109-124.

Fornari, D. J., Peterson, D. W., Lockwood, J. P., Malahoff, A., and Heezen, B. C., 1979, Submarine extension of the southwest rift zone of Mauna Loa volcano, Hawaii; Visual observations from U.S. navy deep submergence vehicle DSV Sea Cliff: Geological Society of America Bulletin, v. 90 (5), 435-443.

Garcia, M. O., Caplan-Auerbach, J., De Carlo, E. H., Kurz, M. D., and Becker, N., 2006, Geology, geochemistry and earthquake history of Lō‘ihi Seamount, Hawai‘i’s youngest volcano: Chemie der Erde, v. 66 (2), 81-108, doi:10.1016/j.chemer.2005.09.002.

Garcia, M. O., and Davis, M. G., 2001, Submarine growth and internal structure of ocean island volcanoes based on submarine observations of Mauna Loa volcano, Hawaii: Geology, v. 29 (2), 163-166, doi:10.1130/0091-7613(2001)029.

Garcia, M. O., Hulsebosch, T. P., and Rhodes, J. M., 1995, Olivine-rich submarine basalts from the southwest rift zone of Mauna Loa volcano; Implications for magmatic processes and geochemical evolution, *in* Rhodes, J. M., and Lockwood, J. P., eds., Mauna Loa Revealed: Structure, Composition, History, and Hazards: American Geophysical Union Geophysical Monograph 92, 219-239.

Gregg, T. K. P., Smith, D. K., 2003, Volcanic investigations of Puna Ridge, Hawai‘i; Relations of lava flow morphologies and underlying slopes: Journal of Volcanology and Geothermal Research, v. 126 (1-2), 63-77, doi:10.1016/S0377-0273(03)00116-1.

Groome, M. G., Gutmacher, C. E., and Stevenson, A. J., 1997, Atlas of GLORIA sidescan-sonar imagery of the Exclusive Economic Zone of the United States; EEZ-View: U.S. Geological Survey Open-File Report 97-540,

URL:http://pubs.usge.gov/of/of97-540/ (accessed August 2007).

Hill, D. P., and Zucca, J. J., 1987, Geophysical constraints on the structure of Kilauea and Mauna Loa volcanoes and some implications for seismomagmatic processes: U. S. Geological Survey Professional Paper 1350, v. 2, 903-917.

Holcomb, R. T., and Robinson, J. E., 2004, Maps of Hawaiian Islands exclusive economic zone interpreted from GLORIA sidescan-sonar imagery: U.S. Geological Survey Scientific Investigation Map Series 2824, scales 1:2,000,000 and 1:4,000,000, 1 sheet, URL: http://pubs.usgs.gov/sim/2004/2824/ (accessed June 2007).

Imbrie, J., Hays, J. D., Martinson, D. G., McIntyre, A., Mix, A. C., Morley, J. J., Pisias, N. G., Prell, W. L., Shackleton, N. J., 1984, The orbital theory of Pleistocene climate; Support from a revised chronology of the marine d^{18}O record, *in* Berger, A. L., Imbrie, J., Hays, J. D., Kukla, G., Saltzman, B, eds., Milankovitch and Climate, Part 1, Reidel, Dordrecht, 269-305.

Jicha, B. R., Rhodes, J. M., Singer, B. S., and Garcia, M. O., 2012, ^{40}Ar/^{39}Ar geochronology of submarine Mauna Loa volcano, Hawaii: Journal of Geophysical Research, v. 117, B09204, doi: 10.1029/2012JB009373.

Kongsberg Maritime, 2003, EM 300 30 kHz multibeam echo sounder for depths reaching 5000 meters, product specification report, Horten, Norway, URL: http://www.whoi.edu/cms/files/instruments/2006/9/160765ad_EM300_Product_specific_lr_13565.pdf, (accessed August 2007).

Lipman, P. W., 1980, The southwest rift zone of Mauna Loa; Implications for structural evolution of Hawaiian volcanoes: American Journal of Science, v. 280-A, 752-776.

Lipman, P. W., 1995, Declining growth of Mauna Loa during the last 100,000 years; Rates of lava accumulation vs. gravitational subsidence, *in* Rhodes, J. M., and Lockwood, J. P., eds., Mauna Loa Revealed: Structure, Composition, History, and Hazards: American Geophysical Union Geophysical Monograph 92, 45-80.

Lipman, P. W., and Coombs, M. L., 2006, North Kona slump; Submarine flank failure during the early(?) tholeiitic shield stage of Hualalai volcano: Journal of

Volcanology and Geothermal Research, v. 151 (1-3), 189-216, doi:10.1016/j.jvolgeores.2005.07.029.

Lipman, P. W., Eakins, B. W., Yokose, H., 2003, Ups and downs on spreading flanks of ocean-island volcanoes; Evidence from Mauna Loa and Kīlauea: Geology, v. 31 (10), 841-844, doi:10.1130/G19745.1.

Lipman, P. W., Normark, W. R., Moore, J. G., Wilson, J. B., and Gutmacher, C. E., 1988, The giant submarine Alika debris slide, Mauna Loa, Hawaii: Journal of Geophysical Research, v. 93 (B5), 4279-4299, doi:10.1029/JB093iB05p04279.

Lipman, P. W., Rhodes, J. M., and Dalrymple, G. B., 1990, The Ninole Basalt; Implications for the structural evolution of Mauna Loa volcano, Hawaii: Bulletin of Volcanology, v. 53 (1), 1-19.

Lipman, P. W., Sisson, T. W., Coombs, M. L., Calvert, A. T., and Kimura, J. I., 2006, Piggyback tectonics; Long-term growth of Kilauea on the south flank of Mauna Loa: Journal of Volcanology and Geothermal Research, v. 151 (1-3), 73-108, doi:10.1016/j.jvolgeores.2005.07.032

Lipman, P. W., and Swenson, A., 1984, Generalized geologic map of the southwest rift zone of Mauna Loa volcano, Hawaii: U.S. Geological Survey Miscellaneous Investigations Series Map I-1323, scale 1:100,000, 1 sheet.

Lockwood, J. P., 1995, Mauna Loa eruptive history; The preliminary radiocarbon record, *in* Rhodes, J. M., and Lockwood, J. P., eds., Mauna Loa Revealed: Structure, Composition, History, and Hazards: American Geophysical Union Geophysical Monograph 92, 81-94.

Lockwood, J. P., and Lipman, P. W., 1987, Holocene eruptive history of Mauna Loa volcano: U.S. Geological Survey Professional Paper 1350, v. 1, 509-535.

Lonsdale, P., 1989, A geomorphological reconnaissance of the submarine part of the East Rift Zone of Kilauea volcano, Hawaii: Bulletin of Volcanology, v. 51 (2), 123-144.

Macdonald, G. A., Abbott, A. T., and Peterson, F. L., 1983, Volcanoes in the sea; The geology of Hawaii, 2nd ed: Honolulu, University of Hawaii Press, 517 p.

Mark, R. K., and Moore, J. G., 1987, Slopes of the Hawaiian Ridge, *in* Decker, R. W.,

Wright, T. L., and Stauffer, P. H., eds., U.S. Geological Survey Professional Paper 1350, v. 1, 101-107.

McMurtry, G. M., Herrero-Bervera, E., Cremer, M. D., Smith, J. R., Resig, J., Sherman, C. E., Torresan, M. E., 1999, Stratigraphic constraints on the timing and emplacement of the Alika 2 giant Hawaiian submarine landslide: Journal of Volcanology and Geothermal Research, v. 94 (1-4), 35-58.

McMurtry, G. M., Watts, P., Fryer, G. J., Smith, J. R., Imamura, F., 2004, Giant landslides, mega-tsunamis, and paleo-sea level in the Hawaiian Islands: Marine Geology, v. 203 (3-4), 219-233, doi:10.1016/S0025-3227(03)00306-2.

Moore, J. G., 1987, Subsidence of the Hawaiian Ridge, *in* Decker, R. W., Wright, T. L., Stauffer, P. H., eds., U.S. Geological Survey Professional Paper 1350, v. 1, 85-100.

Moore, J. G., Bryan, W. B., Beeson, M. H., and Normark, W. R., 1995, Giant blocks in the South Kona landslide, Hawaii: Geology, v. 23 (2), 125-128, doi:10.1130/0091-7613(1995)023.

Moore, J. G., and Chadwick, W. W., 1995, Offshore geology of Mauna Loa and adjacent area, Hawaii, *in* Rhodes, J. M., and Lockwood, J. P., eds., Mauna Loa Revealed: Structure, Composition, History, and Hazards: American Geophysical Union Geophysical Monograph 92, 21-44.

Moore, J. G., and Clague, D. A., 1992, Volcanic growth and evolution of the Island of Hawaii: Geological Society of America Bulletin, v. 104 (11), 1471-1484, doi:10.1130/0016-7606(1992)104.

Moore, J. G., Clague, D. A., Holcomb, R. T., Lipman, P. W., Normark, W. R., and Torrensan, M. E., 1989, Prodigious submarine landslides on the Hawaiian Ridge: Journal of Geophysical Research, v. 94 (B12), 17,465-17,484, doi:10.1029/JB094iB12p17465.

Moore, J. G., Normark, W. R., and Holcomb, R. T., 1994, Giant Hawaiian landslides: Annual Review of Earth and Planetary Sciences, v. 22, 119-144.

Moore, J. G., Normark, W. R., and Szabo, B. J., 1990, Reef growth and volcanism on the submarine southwest rift zone of Mauna Loa, Hawaii: Bulletin of Volcanology, v.

52 (5), 375-380.

Montaggioni, L. F., Cabioch, G., Camoin, G. F., Bard, E., Laurenti, A. R., Faure, G., Déjardin, P., and Récy, J., 1997, Continuous record of reef growth over the past 14 k.y. on the mid-Pacific island of Tahiti: Geology, v. 25 (6), 555-558, doi:10.1130/0091-7613(1997)025.

Morgan, J. K., Moore, G. F., and Clague, D. A., 2003, Slope failure and volcanic spreading along the submarine south flank of Kilauea volcano, Hawaii: Journal of Geophysical Research, v. 108 (B9), doi:10.1029/2003JB002411.

Parfitt, E. A., Gregg, T. K. P., and Smith, D. K., 2002, A comparison between subaerial and submarine eruptions at Kilauea volcano, Hawaii; Implications for the thermal viability of lateral feeder dikes: Journal of Volcanology and Geothermal Research, v. 113 (1-2), 213-242.

Peltier, W. R., 2002, On eustatic sea level history; Last glacial maximum to Holocene: Quaternary Science Reviews, v. 21 (1-3), 377-396.

Pressling, N., Trusdell, F. A., and Gubbins, D., 2009, New and revised (super 14) C dates for Hawaiian surface lava flows; Paleomagnetic and geomagnetic implications: Geophysical Research Letters, v. 36 (11), L11306, doi:10.1029/2009GL037792.

Ren, Z., Takahashi, E., Orihashi, Y., and Johnson, K. T. M., 2004, Petrogenesis of tholeiitic lavas from the submarine Hana Ridge, Haleakala volcano, Hawaii: Journal of Petrology, v. 45 (10), 2067-2099, doi:10.1093/petrology/egh076.

Robinson, J. E., and Eakins, B. W., 2006, Calculated volumes of individual shield volcanoes at the young end of the Hawaiian Ridge: Journal of Volcanology and Geothermal Research, v. 151 (1-3), 306-317, doi:10.1016/j.jvolgeores.2005.07.033.

Rowland, S. K., and Garbeil, H., 2000, Slopes of oceanic basalt volcanoes, *in* Mouginis-Mark, P. J., Crisp, J. A., and Fink, J. H., eds., Remote sensing of active volcanism: American Geophysical Union Geophysical Monograph 116, 223-247.

Sansone, F. J., and Smith, J. R., Rapid mass wasting following nearshore submarine volcanism on Kilauea volcano, Hawaii: Journal of Volcanology and Geothermal Research, v. 151 (1-3), 133-139, doi:10.1016/j.jvolgeores.2005.07.026.

Sherrod, D. R., Sinton, J. M, Watkins, S. E., and Brunt, K. M., 2007, Geologic map of the State of Hawai‘i: U. S. Geological Survey Open-File Report 2007-1089, 85 p., 8 sheets, URL: http://pubs.usgs.gov/of/2007/1089/.

Smith, D. K., Kong, L. S. L., Johnson, K. T. M., and Reynolds, J. R., 2002, Volcanic morphology of the submarine Puna Ridge, Kilauea volcano, *in* Takahashi, E., Lipman, P. W., Garcia, M. O., Naka, J., and Aramaki, S., eds., Hawaiian Volcanoes: Deep Underwater Perspectives: American Geophysical Union Geophysical Monograph 128, 125-142.

Smith, J. R., Satake, K., Morgan, J. K., and Lipman, P. W., 2002, Submarine landslides and volcanic features on Kohala and Mauna Kea volcanoes and the Hana Ridge, Hawaii, *in* Takahashi E., Lipman, P. W., Garcia, M. O., Naka, J., and Aramaki, S., eds., Hawaiian Volcanoes: Deep Underwater Perspectives: American Geophysical Union Geophysical Monograph 128, 11-28.

Stearns, H. T., and Clark, W. O., 1930, Geology and water resources of the Kau District, Hawaii (including part of Kilauea and Mauna Loa volcanoes: U.S. Geological Survey Water-Supply Paper, Report W 0616, 194 p.

Stearns, H. T., and Macdonald, G. A., 1946, Geology and ground-water resources of the Island of Hawaii: Hawaii Division of Hydrography Bulletin 9, 363 p.

Torresan, M. E., Gardner, J. V., 2000, Acoustic mapping of the regional seafloor geology in and around Hawaiian ocean dredged-material disposal sites: U. S. Geological Survey Open-File Report 00-0124, 63 p., 8 sheets, URL: http://geopubs.wr.usgs.gov/open-file/of00-124/.

Trusdell, F. A., 1995, Lava flow hazards and risk assessment on Mauna Loa volcano, Hawaii, *in* Rhodes, J. M., and Lockwood, J. P., eds., Mauna Loa Revealed: Structure, Composition, History, and Hazards: American Geophysical Union Geophysical Monograph 92, 327-336.

Trusdell, F.A., 2012, Mauna Loa; History, hazards, and risk of living with the world’s largest volcano: U.S. Geological Survey Fact Sheet 2012–3104, 4 p. URL: http://pubs.usgs.gov/fs/2012/3104/fs2012-3104.pdf.

Trusdell, F.A., and Lockwood, J.P., 2006, Geologic Map of the Northeast Flank of

Mauna Loa Volcano, Island of Hawai‘i, Hawaii: U.S. Geological Survey SIM 2932-A, scale 1:50,000, in press.

Trusdell, F.A., and Lockwood, J.P., 2009, Geologic Map of the Central Southeast Flank of Mauna Loa Volcano, Island of Hawai‘i, Hawaii: U.S. Geological Survey SIM 2932-B, scale 1:50,000, in press.

Trusdell, F. A., Wolfe, E. W., and Morris, J., 2006, Digital database of the geological map of the Island of Hawai‘i: U.S. Geological Survey Data Series 144, 18p, 1 sheet. URL: http://pubs.usgs.gov/ds/2005/144/ (accessed July 2007).

Walker, G. P. L., 1990, Geology and volcanology of the Hawaiian Islands: Pacific Science, v. 44 (4), 315-347.

Wanless, V. D., Garcia, M. O., Trusdell, F. A., Rhodes, J. M., Norman, M. D., Weis, D., Fornari, D. J., Kurz, M. D., and Guillou, H., 2006, Submarine radial vents on Mauna Loa volcano, Hawai‘i: Geochemistry, Geophysics, Geosystems, v. 7 (5), Q05001, doi: 10.1029/2005GC001086.

Webster, J. M., Clague, D. A., Riker-Coleman, K., Gallup, C., Braga, J. C., Potts, D., Moore, J. G., Winterer, E. L., and Paull, C. K., 2004, Drowning of the -150 m reef off Hawaii; A casualty of global meltwater pulse 1A?: Geology, v. 32 (3), 249-252, doi:10.1130/G20170.1.

Wolfe, E. W., and Morris, J., 1996, Geologic map of the Island of Hawaii: U.S. Geological Survey Miscellaneous Investigations Series Map I-2524-A, scale 1:100,000, 18p. 3 sheets.

Woods Hole Oceanographic Institution (WHOI), URL: http://www.whoi.edu/science/instruments; http://4dgeo.whoi.edu/jason (accessed 2007).

Yokose, H., and Lipman, P. W., 2004, Emplacement mechanisms of the South Kona slide complex, Hawaii Island; Sampling and observations by remotely operated vehicle Kaiko: Bulletin of Volcanology, v. 66 (7), 569-584, doi:10.1007/s00445-004-0339-9.

Zucca, J. J., Hill, D. P., and Kovach, R. L., 1982, Crustal structure of Mauna Loa volcano, Hawaii, from seismic refraction and gravity data: Bulletin of

Seismological Society of America, v. 72 (5), 1535-1550.